AD-A174 916 INVESTIGATION OF SURFACE PHENOMENA IN THERMIONIC ENERGY CONVERSION(U) OREGON GRADUATE CENTER BEAVERTON DEPT OF APPLIED PHYSICS AND E... P R DAVIS 01 OCT 86 1/1

UNCLASSIFIED AFOSR-TR-86-2100 AFOSR-83-0105 F/G 7/4 NL

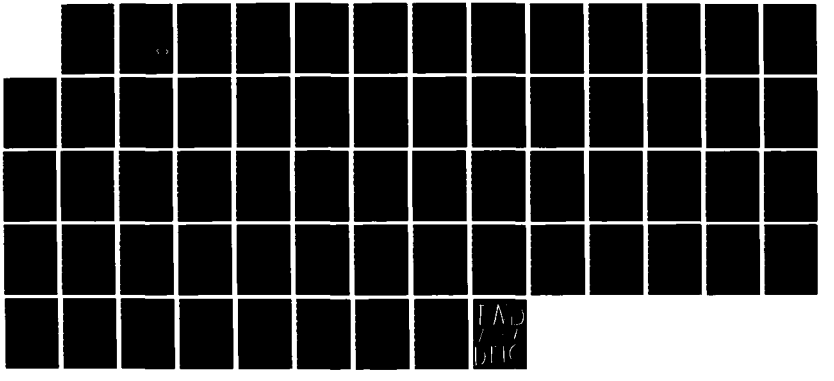

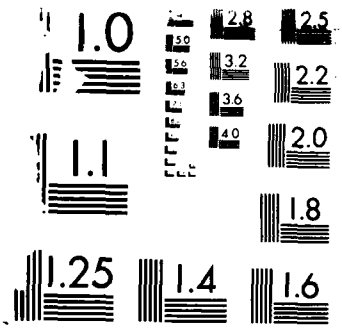

RESOLUTION TEST CHART

(2)

AFOSR-TR- 86-2100

INVESTIGATION OF SURFACE PHENOMENA IN THERMIONIC ENERGY CONVERSION

Final Technical Report

For the Period

1 March 1983 - 31 July 1986

By

P. R. Davis

Oregon Graduate Center

19600 N. W. Von Neumann Drive

Beaverton, OR 97006

1 October 1986

Prepared for:

Air Force Office of Scientific Research

Bolling AFB

Washington, DC 20332

Unclassified

SECURITY CLASSIFICATION OF THIS PAGE

REPORT DOCUMENTATION PAGE

1a. REPORT SECURITY CLASSIFICATION Unclassified	1b. RESTRICTIVE MARKINGS
2a. SECURITY CLASSIFICATION AUTHORITY	3. DISTRIBUTION/AVAILABILITY OF REPORT Approved for public release; distribution unlimited
2b. DECLASSIFICATION/DOWNGRADING SCHEDULE	
4. PERFORMING ORGANIZATION REPORT NUMBER(S)	5. MONITORING ORGANIZATION REPORT NUMBER(S) AFOSR-TR- 86-2100
6a. NAME OF PERFORMING ORGANIZATION Oregon Graduate Center 6b. OFFICE SYMBOL (If applicable)	7a. NAME OF MONITORING ORGANIZATION AFOSR/NC
6c. ADDRESS (City, State and ZIP Code) Dept of Applied Physics & Electrical Engr Beaverton, OR 97006	7b. ADDRESS (City, State and ZIP Code) Bldg 410 Bolling AFB DC 20332-6448
8a. NAME OF FUNDING/SPONSORING ORGANIZATION AFOSR 8b. OFFICE SYMBOL (If applicable) NC	9. PROCUREMENT INSTRUMENT IDENTIFICATION NUMBER AFOSR-83-0105
8c. ADDRESS (City, State and ZIP Code) Bldg 410 Bolling AFB DC 20332-6448	10. SOURCE OF FUNDING NOS. PROGRAM ELEMENT NO. 61103F; PROJECT NO. 2303; TASK NO. A2; WORK UNIT NO.
11. TITLE (Include Security Classification) Investigation of Surface Phenomena In Thermionic Energy Conversion	
12. PERSONAL AUTHOR(S) P. R. Davis	
13a. TYPE OF REPORT Final 13b. TIME COVERED FROM 830301 TO 860631	14. DATE OF REPORT (Yr., Mo., Day) 86 10 01 15. PAGE COUNT 60
16. SUPPLEMENTARY NOTATION	
17. COSATI CODES FIELD / GROUP / SUB. GR.	18. SUBJECT TERMS (Continue on reverse if necessary and identify by block number) Surface, Thermionic, LaB_6, Oxygen

19. ABSTRACT (Continue on reverse if necessary and identify by block number)

The general goal of this project has been to enhance the understanding of surface phenomena related to thermionic energy conversion (TEC), in particular, surface properties of electrode materials which have the potential of enhancing significantly the performance of practical devices for advanced mode TEC. A variety of surface analysis techniques has been used in the study of these surfaces. A major part of the research effort has been devoted to study of clean surface properties of LaB_6 single crystals. Investigations of residual gas interactions with low work function emitter surfaces has been directed toward the study of O2 interactions with low work function single crystal faces of LaB_6. Measurements were made on both the clean and oxidized LaB_6 surfaces using Auger electron spectroscopy (AES) and x-ray photoelectron spectroscopy (XPS) and quadrupole mass spectrometry (QMS) for analysis of the desorbing molecular species. The nature of the surface oxide species were correlated with thermal evaporation characteristics. The coadsorption of Zr and oxygen

20. DISTRIBUTION/AVAILABILITY OF ABSTRACT UNCLASSIFIED/UNLIMITED ☒ SAME AS RPT. ☒ DTIC USERS ☐	21. ABSTRACT SECURITY CLASSIFICATION Unclassified
22a. NAME OF RESPONSIBLE INDIVIDUAL LARRY W. BURGGRAF, Lt Col, USAF	22b. TELEPHONE NUMBER (Include Area Code) (202) 767-4960 22c. OFFICE SYMBOL NC

DD FORM 1473, 83 APR EDITION OF 1 JAN 73 IS OBSOLETE

SECURITY CLASSIFICATION OF THIS PAGE

onto W causes a lowering of the work function of the (100) crystal plane from 4.7 to 2.6 eV. The resulting surface is remarkably stable and has practical application as a cathode for fine-focussed beam applications.

I. Introduction

The general goal of this project has been to enhance the understanding of surface phenomena related to thermionic energy conversion (TEC). In particular, we have investigated surface properties of electrode materials which have the potential of enhancing significantly the performance of practical devices for advanced mode TEC. In large part, this effort has been devoted to the study of surface properties of materials which exhibit inherently low work functions.

A. Thermionic energy conversion background

Thermionic energy conversion represents an attractive means of providing low-voltage electrical power for space systems and for various terrestrial applications. A TEC device consists of a close-spaced Cs-vapor diode with a heated electron emitter and a cooled electron collector. The work function difference between emitter and collector (with adsorbed Cs) provides the necessary output voltage, and a high electron current density is provided by the hot emitter. The attractiveness of TEC for space applications rests in the flexibility of the converter with respect to its heat source, its high power density compared with competing technologies and its high waste heat rejection temperature, essential for efficient spacecraft cooling. A more detailed discussion of TEC considerations may be found in an article we have published recently [1].

B. Research approach

The objective of this research effort has been to study materials which may make TEC device operation more efficient in the range of temperatures suitable for space applications (up to about 1800K for the emitter and 900K or less for the collector). This goal of more efficient TEC devices requires so-called advanced mode operation, with Cs pressures much

lower than about 1 torr, a value typical of ignited-mode converters which represent the present state of the art. Advanced-mode devices demand emitter and collector surfaces which either have inherently low work functions or which adsorb Cs so strongly as to maintain low work functions at elevated temperatures even in extremely low Cs pressures. A primary emphasis of our research has been the study of candidate emittter materials for advanced TEC, that is, the study of clean low work function surfaces and their interactions with residual gases.

A variety of surface analysis techniques has been used in the study of these surfaces. These techniques and the results they provide are summarized in Table I. Some of these analytical tools are located in our group at the Oregon Graduate Center. However, we have also used facilities of the NSF Center for Research in Surface Science (CRISS) located at Montana State University, Bozeman, MT. Both XPS and SAM experiments have been performed at CRISS, and these experiments have provided information crucial to the understanding of surface properties of TEC electrode materials. The cost of use of the CRISS equipment is essentially travel and per diem expenses, making these studies extremely cost effective.

C. Specific project goals

Table II summarizes the goals of this research project. the breakdown into specific research tasks is done in such a way that direct correlation may be made with Section II of this report, "Accomplishments of the Research Effort."

TABLE I

SURFACE ANALYSIS TECHNIQUES

Analysis Technique	Type of Data Provided	TEC Electrode Information
AES	Elemental composition of top 2-3 atomic layers	Amount of cesium, oxygen, contaminants on surface
SAM (Scanning AES)	AES with lateral imaging of surface; surface composition, uniformity; resolution ≈ 500 Å	Distribution of elements across surface; non-uniform surface studies (textured, polycrystalline, composite)
XPS (ESCA)	Chemical environment of each surface atom species; broad area analysis; relative positions of surface atoms (in angle resolved mode)	Nature of chemical bonding of surface atoms, within the clean surface and to adsorbed atoms; atomic positions
SIMS	Composition of first atomic layer; depth profiling; extreme sensitivity for minority component detection	Composition of first atomic layer; bulk distribution of major elements and contaminants in the near-surface region
LEELS	Vibration frequencies of surface atoms (surface sensitive analog of infrared spectroscopy)	Nature of surface chemical bonds
FERP	Absolute surface work function; electron reflection characteristics in 0-20 eV range	Electrode work function; electron reflection characteristics
TDS	Identification of thermal desorption products as function of temperature	Clean surface thermal stability; bond energies of adsorbed cesium, oxygen and contaminants
FEM	Diffusion coefficients of adsorbed layers or self diffusion of clean surfaces; work function of single crystal plane	Kinetics of two-dimensional motion of surface atoms
FIM	Atomic arrangement of surface atoms	Role of substrate atomic structure

TABLE II

SUMMARY OF RESEARCH GOALS

TASK I: Investigation of clean low work function emitter surfaces

- A. Rare earth hexaboride single crystals
- B. The Zr/O/W(100) system
- C. Group IVB carbides

Task II: Investigation of residual gas interactions with low work function emitter surfaces

Task III: Investigations of collector surfaces

- A. Clean Mo-oxide
- B. Mo-oxide with adsorbed Cs

Task IV: Construction and use of *in situ* analysis system

Task V: Construction and use of angle-resolved Auger electron spectroscopy system (ARAES)

II. Accomplishments of the Research Effort

A. Task I(A): Investigations of clean surface properties of rare earth hexaboride single crystals

A major part of the research effort has been devoted to the study of clean surface properties of LaB_6 single crystals. Surface electronic, structural and thermal stability characteristics have been investigated for a variety of precisely known material stoichiometries and crystal faces. The $LaB_{6.09}$(310) surface has proved to exhibit the best electron emission capabilities consistent with low material volatility in the temperature range of interest for TEC emitter electrodes. This surface has a measured effective thermionic work function of 2.45 eV at 1600K, yielding approximately 10 A/cm^2 electron emission with a material evaporation rate less than 5×10^{-11} $g/cm^2/sec$. These studies have been thoroughly discussed in the literature [1-5].

B. Task I(B): Studies of the Zr/O/W(100) low work function surface

The coadsorption of Zr and oxygen onto W causes a lowering of the work function of the (100) crystal plane from 4.7 to 2.6 eV [6-8]. The resulting surface is remarkably stable and has practical application as a cathode for fine-focussed beam applications. It also may be useful as a TEC emitter material. We have investigated the properties of this surface using Auger electron spectroscopy, thermal desorption mass spectrometry, thermionic and retarding potential work function measurement techniques and field emission methods. The results of these investigations have been published in the open literature [9-11]. We have also very recently used XPS to study the chemical state of adsorbed Zr in the low work function configuration of this surface. In these studies, we have been able to identify a Zr oxidation state intermediate between ZrO and Zr^{2+} which we identify with the low work function

identify with the low work function surface. We associate this state with a Zr-O positive surface dipole, which most likely has the O atom bonded to the W(100) surface at a four-fold coordination site.

C. Task I(C): Preparation and study of surfaces of group IVB carbide single crystals

This task was not undertaken until late in the project, and represents only a minor portion of the total effort. Nevertheless, the IVB carbides (TiC, ZrC and HfC) exhibit unique properties of stability, inertness and, according to the limited literature on the subject, low work function. Thus, these materials may eventually be of considerable practical importance in advanced mode TEC applications. We have constructed and tested an arc float-zone refinement system for preparing oriented single crystal specimens of the group IVB carbides. Crystals of diameter 1-2 mm can be prepared, using as starting material rods cut from sintered powders of these materials. Hot pressing is a more satisfactory method of producing compact starting materials, especially ZrC, but we have had reasonable success with cold pressed and sintered powders.

As is the case with the rare earth hexaborides, stoichiometry may have considerable effect upon the work functions and volatilities of the crystal specimens. Furthermore, the work function is expected to vary considerably from face to face of the crystal. We have studied carefully the surface properties of a single specimen of ZrC, with (100) orientation and unknown stoichiometry.

The work function of a specimen of a compound material depends strongly upon its surface composition. Any surface exposed to ambient atmosphere must first be cleaned by some means before its surface may be studied, and it is not possible to perform this cleaning step without modifying the original

surface to some extent. The ideal situation would be a specimen which is cleaved in ultrahigh vacuum, presumably yielding a surface with composition the same as that of the bulk material. Even such a surface will change its stoichiometry during heating in the analysis system, however, in response to thermodynamic forces existing at the interface between solid and vacuum. In the present investigation we have studied the properties of a crystal prepared in ambient atmosphere and subsequently cleaned in vacuum by argon ion sputtering and heating. We have studied changes in surface composition as a function of cleaning procedure using AES, and we have measured the corresponding FERP work function changes.

Table III summarizes results of this study. The minimum work function we have observed on the ZrC(100) surface is 3.5 eV, in agreement with an earlier study on this face [12]. We have used both ion sputtering and heating to clean the surface of the specimen. As indicated in Table III, different treatments of the surface produce changes in surface stoichiometry, as indicated by the ratios of C to Zr Auger peaks. The C(KLL) and Zr(MNN) electrons have approximately the same escape depths since their energies are comparable, and changes in their ratio thus represent changes in the C/Zr ratio very near the surface. The Zr(LMM) escape depth is considerably greater, however, so the C(KLL)/Zr(LMM) ratio is a crude measure of the change in surface C content relative to the (fixed) bulk composition. The amounts of contamination are relatively low in the results reported here, so the different work functions shown in Table III seem to be related to changes in surface stoichiometry.

TABLE III

AUGER AND WORK FUNCTION SUMMARY FOR ZrC(100)

Treatment	Ar^+ Sputter	Heat 1300°C_B 30 sec	Heat 1420°C_B 30 sec	Heat 1475°C_B 30 sec
$\frac{C(KLL)}{Zr(MNN)}$ Peak ratio	2.1	2.3	2.4	2.3
$\frac{C(KLL)}{Zr(LMM)}$ Peak ratio	.24	.34	.32	.37
O surface concentration (%)	6	1.4	.8	2.3
N surface concentration (%)	3.6	2.2	1.3	1.6
ϕ (FERP)(eV)	5.00 ± 0.05	3.48 ± 0.05	3.78 ± 0.05	3.57 ± 0.05

The fact that work functions as low as 2.5 eV have been reported for polycrystalline specimens of $ZrC_{0.90}$ bulk stoichiometry [13] suggests two conclusions from the data obtained on our ZrC(100) specimen: 1) the composition of our sample may not be exactly $ZrC_{0.90}$ and 2) the (100) face may not be the lowest work function face of ZrC.

Conclusion 1) results from the difficulty in determining surface/bulk compositions of compound materials which have been cleaned in vacuum. Since it is certain that the bulk and surface compositions differ following the cleaning treatment, what is measured by techniques such as AES is a surface-weighted average over several atomic layers of varying composition. Thus, ratios of AES signals of the different elements in the material yield at best a qualitative indication of the true surface stoichiometry. The precise

bulk stoichiometry of the material cannot be determined at all by AES of these specimens, but is best measured by wet chemical analysis, a destructive procedure. We have not performed such analyses due to the small number of ZrC specimens we have prepared. A careful investigation of the effect of bulk stoichiometry upon the surface properties of ZrC single crystals needs to be carried out, as has been done for LaB_6 [2,14].

Conclusion 2) would be best verified by FEM/FIM studies similar to those performed on LaB_6 [3], or by use of a thermionic emission microscope. Such an investigation would allow the lowest work function (most strongly electron emitting) planes to be identified so that further studies of their surface properties could be made on macroscopic specimens. A program of FEM/FIM research on IVB carbides is currently being pursued by collaborative effort between our group and that of Dr. C. Hinrichs of Linfield College, McMinnville, OR. The Linfield portion of this research has an independent source of funding, and that effort is still in progress. We expect, at some time in the future, to select and study the lowest work function planes of ZrC as determined by FEM studies of the OGC/Linfield collaboration.

D. Task II: Investigations of residual gas interactions with low work function emitter surfaces

Effort on this task has been directed toward the study of O_2 interactions with low work function single crystal faces of LaB_6. Results on the (100) surface have been published in the scientific literature [15]. A very detailed investigation of the O_2-LaB_6(310) interaction was made by K. D. McKinstry of our group as a M. S. research project. The primary results of these studies are discussed in the following paragraphs.

Measurements were made on both the clean and oxidized LaB_6(310) surfaces using Auger electron spectroscopy (AES) and x-ray photoelectron spectroscopy

(XPS) for surface analysis and quadrupole mass spectrometry (QMS) for analysis of the desorbing molecular species. These experimental techniques allowed the acquisition of information on the nature of surface oxide species and their thermal evaporation charcteristics. Experiments performed in fixed pressures of O_2 yielded insight into the formation and removal of various oxide species under conditions similar to actual cathode operation.

Figure 1 is a diagram of the experimental apparatus used for the AES and QMS studies. This setup allowed O_2 pressure and sample temperature to be adjusted as desired while monitoring desorption products or surface composition. XPS measurements were made independently using facilities of the Center for Research in Surface Science (CRISS), an NSF facility housed at Montana State University, Bozeman, MT.

Studies of both adsorption/desorption and steady-state heating in O_2 were performed. In the former case, the sample was first flashed clean in ultra-high vacuum by heating to 1700 K. The sample was then cooled to and held at the temperature desired for adsorption, while oxygen was admitted to the system at controlled pressure for the necessary time by means of a precision leak valve. After adsorption was completed, we pumped down the system to base pressure and ramped the sample temperature while monitoring desorption products (QMS) or surface composition (AES).

Steady-state measurements were made by heating in the required manner while a steady pressure of O_2 was maintained in the system. Ramped-temperature studies were performed slowly to achieve approximately steady-state conditions.

1) Nature of surface oxides

Adsorption of O_2 to saturation at room temperature on the LaB_6(310) surface forms a stable layer of approximately one atomic layer thickness

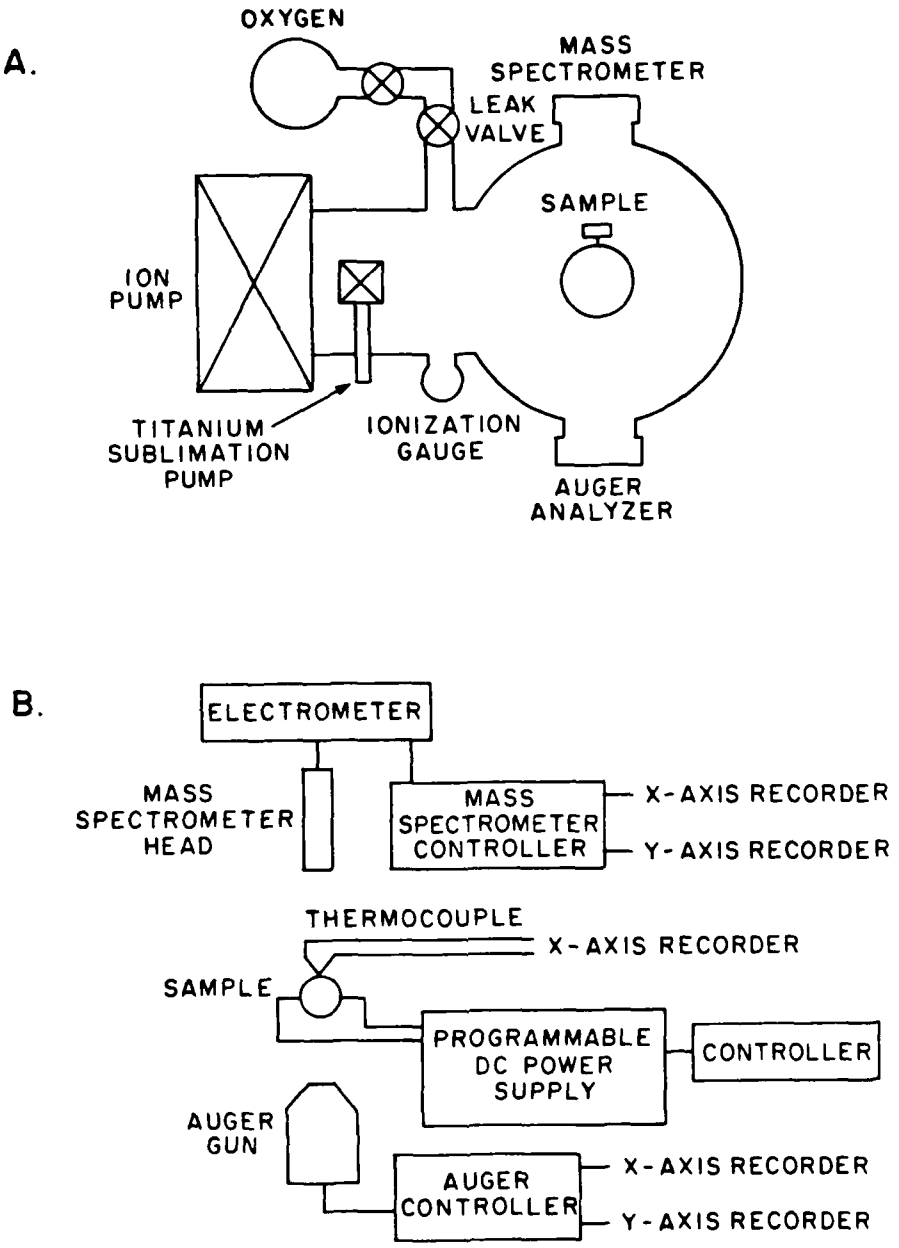

Figure 1. Diagram of the experimental apparatus for $LaB_6(310)$-O_2 interaction studies. Part A: the physical apparatus; part B: the electronics used in conjunction with the physical apparatus.

(monolayer) after an exposure of ~ 50 L. (1 L = 1 Langmuir = 1×10^{-6} torr-sec exposure.) This exposure is more than three times as much as the ~ 15 L required for saturation of the (100), (110), (111) or (210) surfaces [16-18]. This discrepancy may imply a lower sticking coefficient for O_2 onto the (310) surface. In any case, the surface so formed is characteristic of a chemisorbed layer rather than a true oxide, and was not studied in great detail.

Adsorption of O_2 at temperatures of ~ 1000 K or more exhibits a different behavior. More O_2 can be adsorbed at these temperatures than at 300 K, and thick, visible oxide layers can form under certain conditions. In addition, oxidation products can be observed mass spectrometrically in steady-state experiments during the oxidation process (discussed below) and surface faceting occurs. Finally, complex changes in the AES and XPS peak shapes confirm the presence of tightly-bonded oxide species on the surface.

Figure 2 shows AES spectra observed for the clean LaB_6(310) surface and for chemisorbed O_2 and oxidized layers on this surface. Substantial peak shape changes can be seen in both the boron and lanthanum spectra with oxygen present. Qualitatively, one may attribute the differences in these spectra to chemically induced changes in binding energy of the valence electrons involved in the B(KLL) and La(MNN) Auger transitions. Splitting of the La(MNN) peak is a characteristic feature observed whenever O_2 is adsorbed onto LaB_6 surfaces.

Hanke and Muller [19] have studied differences in the shape of the B(KLL) peak in elemental boron, B_4C, BN and B_2O_3. They find that chemical combination of boron with electronegative elements opens additional decay channels for recombination of the boron hole induced to initiate the Auger process. The net result is the formation of a more complicated B(KLL) Auger spectrum when boron acts as the electropositive element of a molecule. The

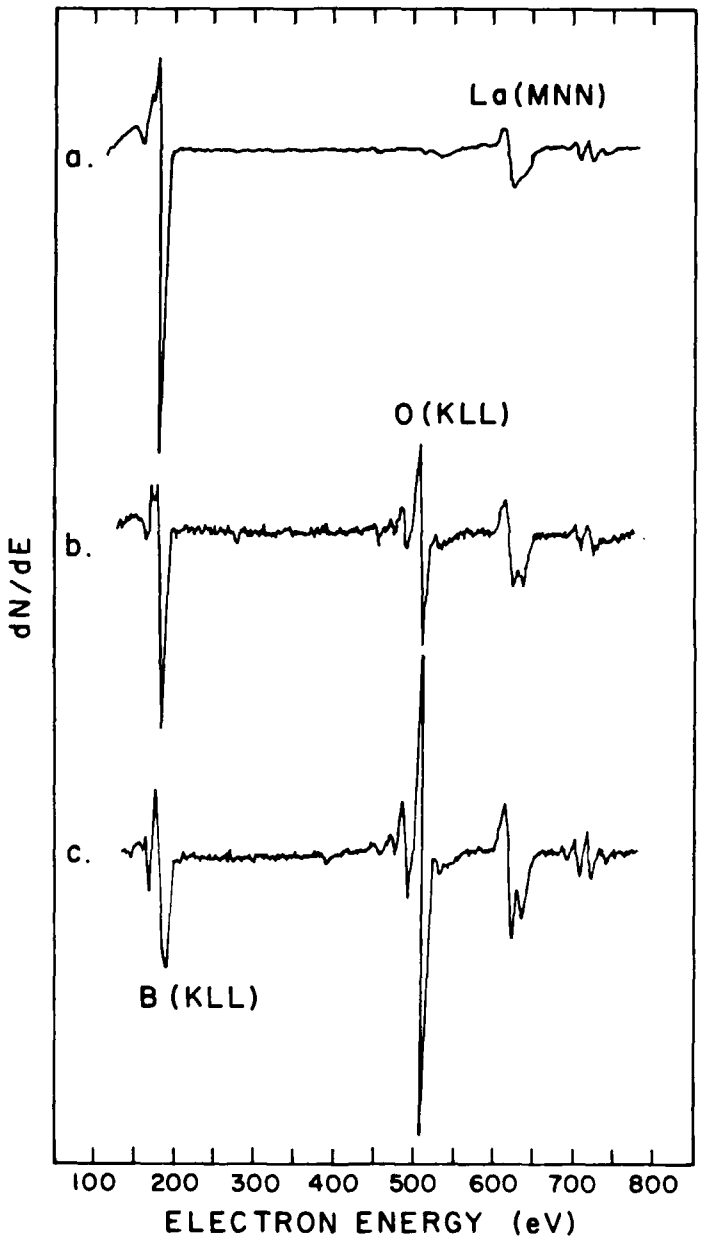

Figure 2. Auger spectra of $LaB_6(310)$ for three different oxidation conditions. Curve a: clean surface; curve b: room temperature oxygen saturation (10^{-4} torr-sec); curve c: fully oxidized surface (1.2×10^{-3} torr-sec at 1600 K).

B(KLL) spectrum we observe for clean LaB_6 is virtually identical to that recorded by Hanke and Muller for pure boron.

The B(KLL) spectrum for oxidized LaB_6, Figure 2(c), is similar to that of B_2O_3. There are significant differences between these latter two spectra, however, suggesting that boron in the oxidized LaB_6(310) surface is not present simply as B_2O_3. Furthermore, one might imagine that the oxygen monolayer spectrum of Figure 2(b) could be formed by a simple superposition of the clean and oxidized LaB_6 spectra of Figures 2(a) and (b), respectively. However, it is not at all clear that this is true. Therefore, we undertook a series of XPS measurements to investigate in more detail the nature of adsorbed oxygen and oxidized layers on the LaB_6(310) surface.

Spectra of LaB_6 with room-temperature adsorbed O_2 and with O_2 adsorbed at 1200 K were measured by XPS. These results were compared with spectra of clean LaB_6, commercial $LaBO_3$ and La_2O_3 formed by oxidation of metallic La in air. The spectrum of B_2O_3 was not measured in this study. We deduce from these results that neither pure $LaBO_3$ nor La_2O_3 is formed by adsorption of O_2 onto LaB_6 at room temperature or at 1200 K. Figures 3-8 compare La3d, B1s and O1s lineshapes for the various surfaces studied. Note the significant differences evident in these spectra. In particular, a comparison of the room-temperature adsorbed O_2 and 1200 K adsorbed O_2 spectra is in order.

The La3d (Figures 3,4) spectra (and La4d, not shown) exhibit peak splitting when O_2 is adsorbed at high temperature, while broad peaks are observed in the clean and room-temperature O_2 adsorbed LaB_6 spectra. Similarly, the O1s spectrum (Figure 6) is much sharper on the surface heated in O_2 than on the room temperature adsorbed oxygen layer. Finally, the B1s spectrum following O_2 adsorption at high temperature has two peaks, separated by ~ 4 eV, while the clean and room-temperature adsorbed spectra show a single

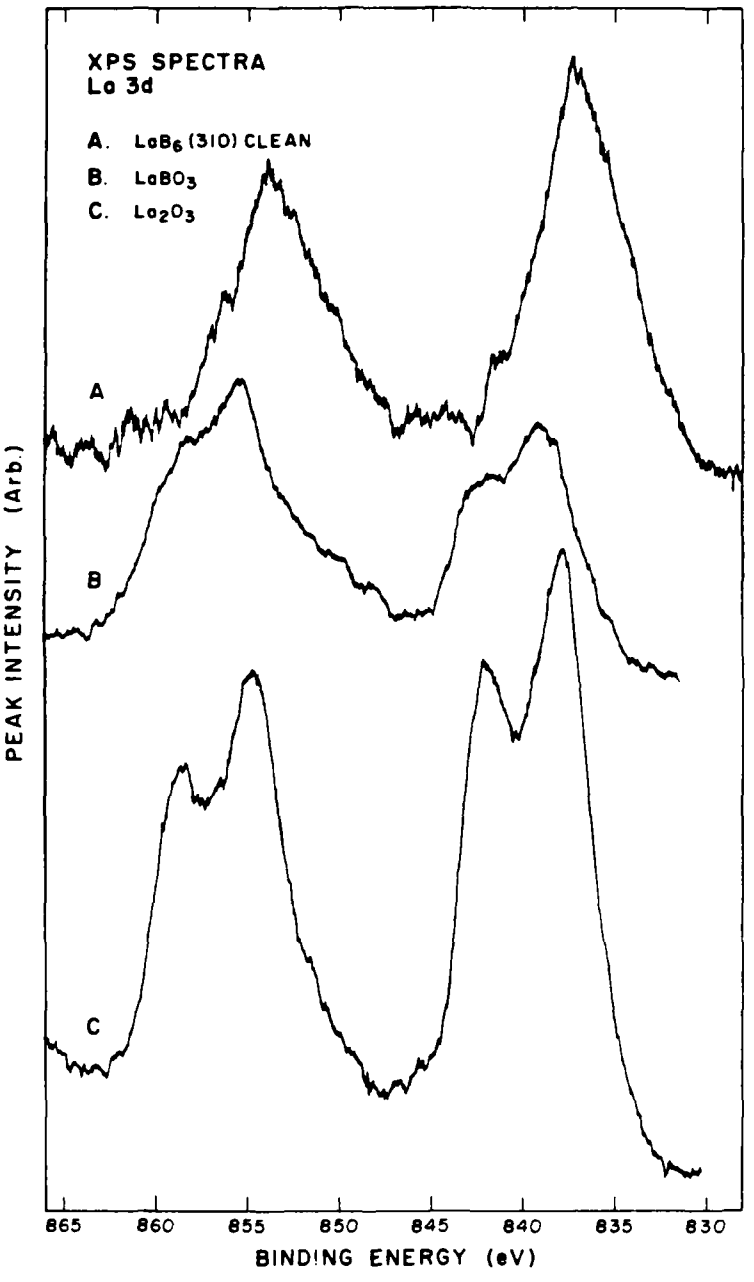

Figure 3. La 3d XPS spectra for clean $LaB_6(310)$, for $LaBO_3$ and for La_2O_3.

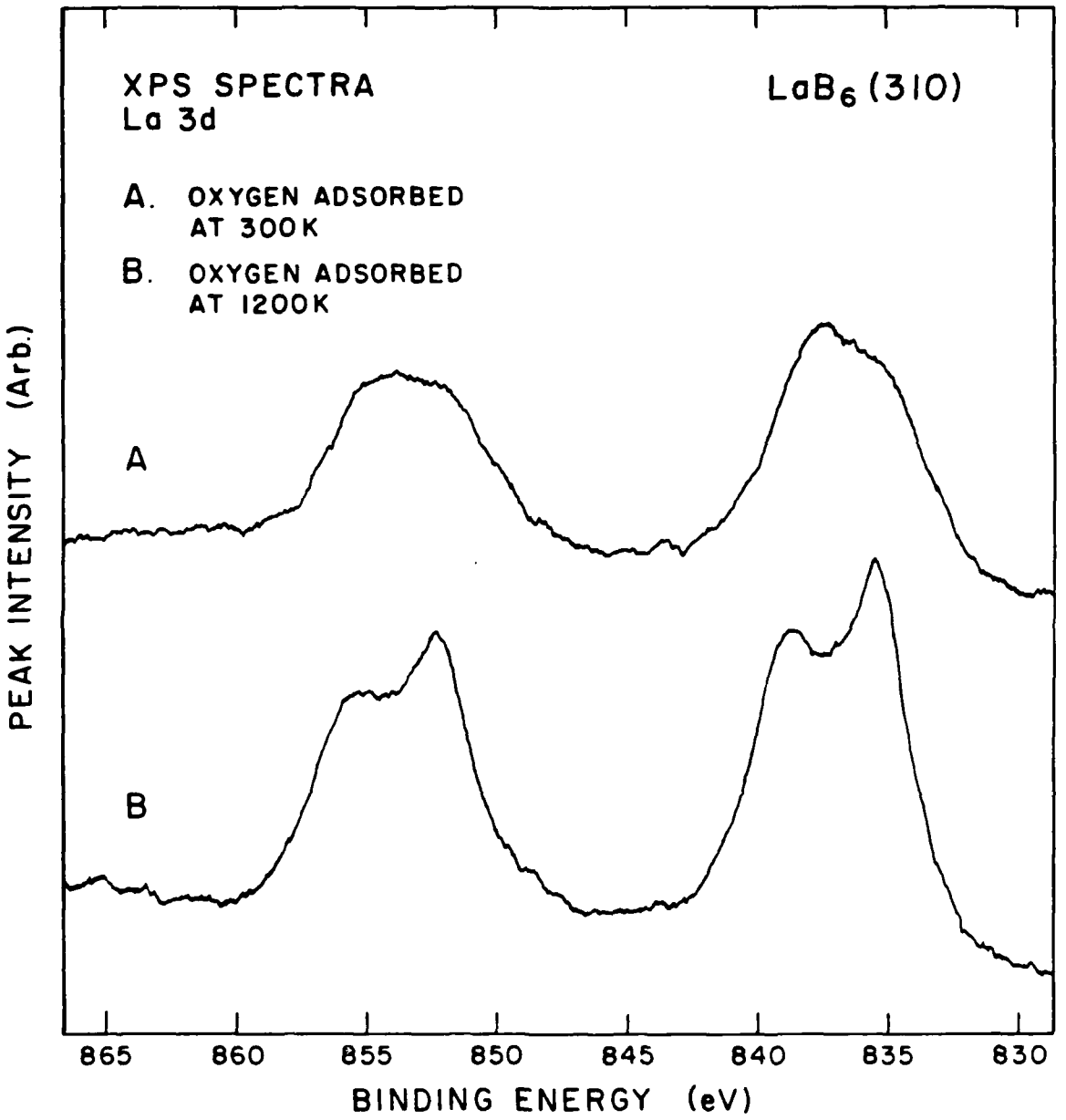

Figure 4. La 3d XPS spectra for LaB_6(310) with oxygen adsorbed at two different temperatures.

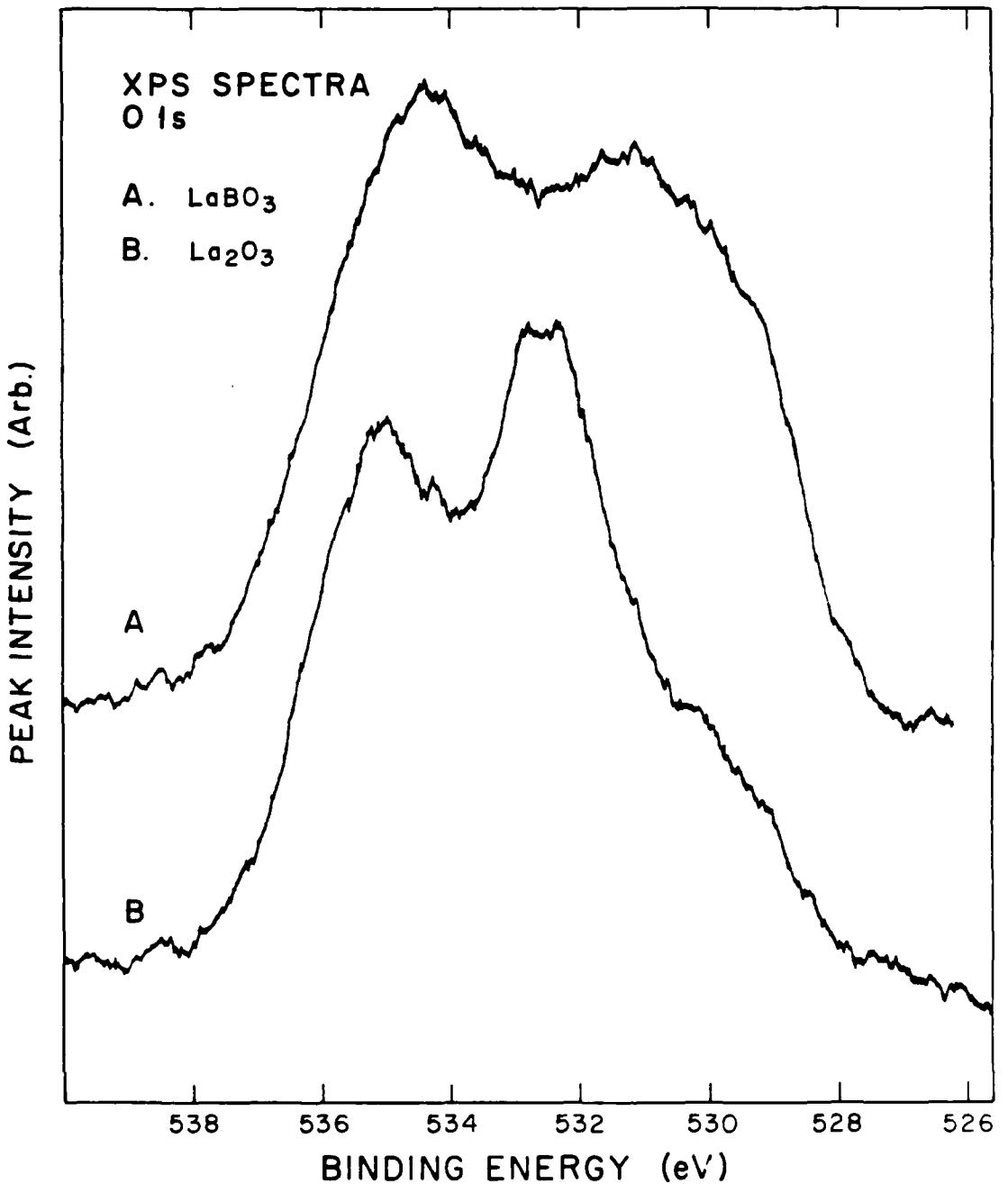

Figure 5. O 1s XPS spectra for $LaBO_3$ and La_2O_3.

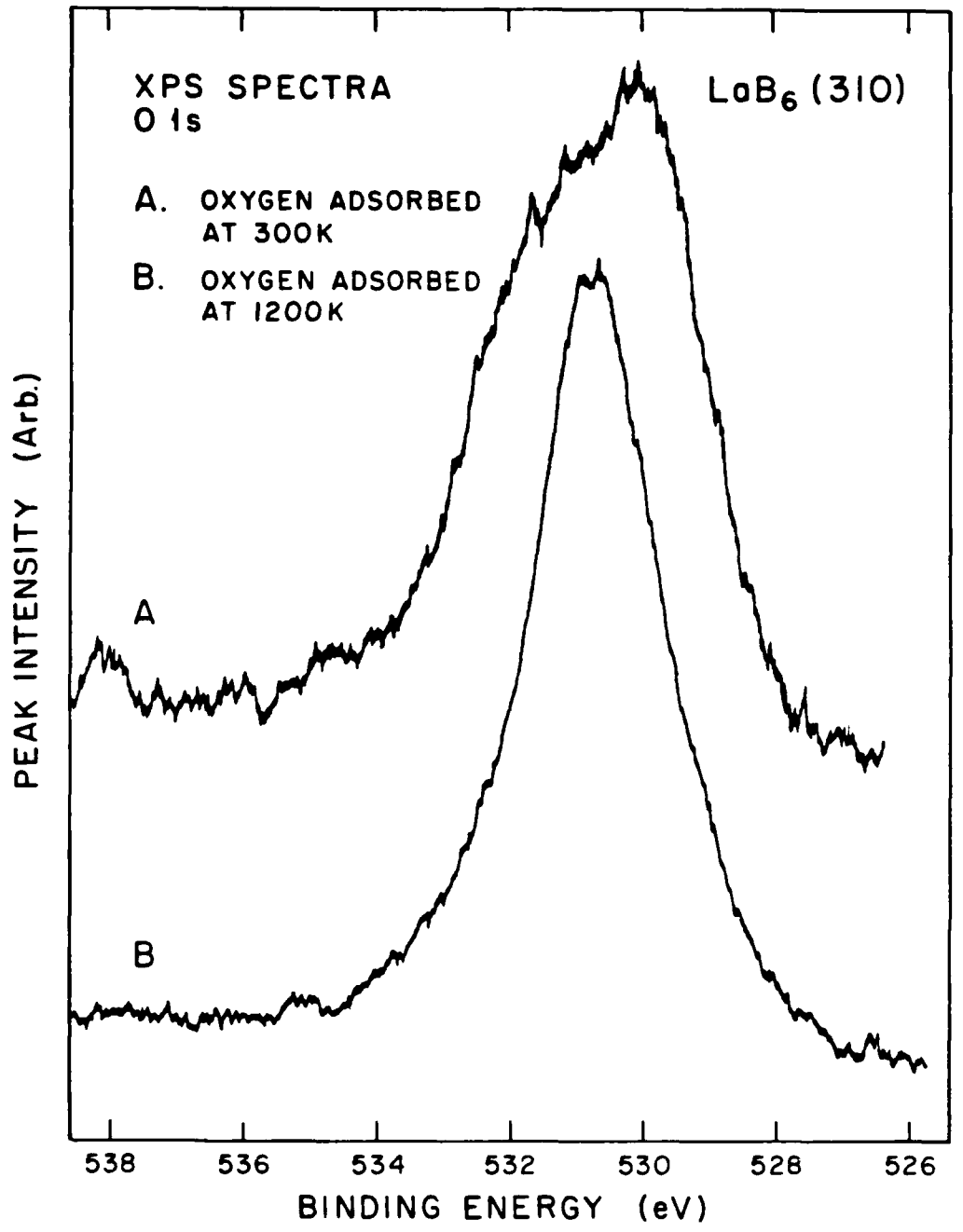

Figure 6. O 1s XPS spectra for O adsorbed onto LaB_6(310) at two different temperatures.

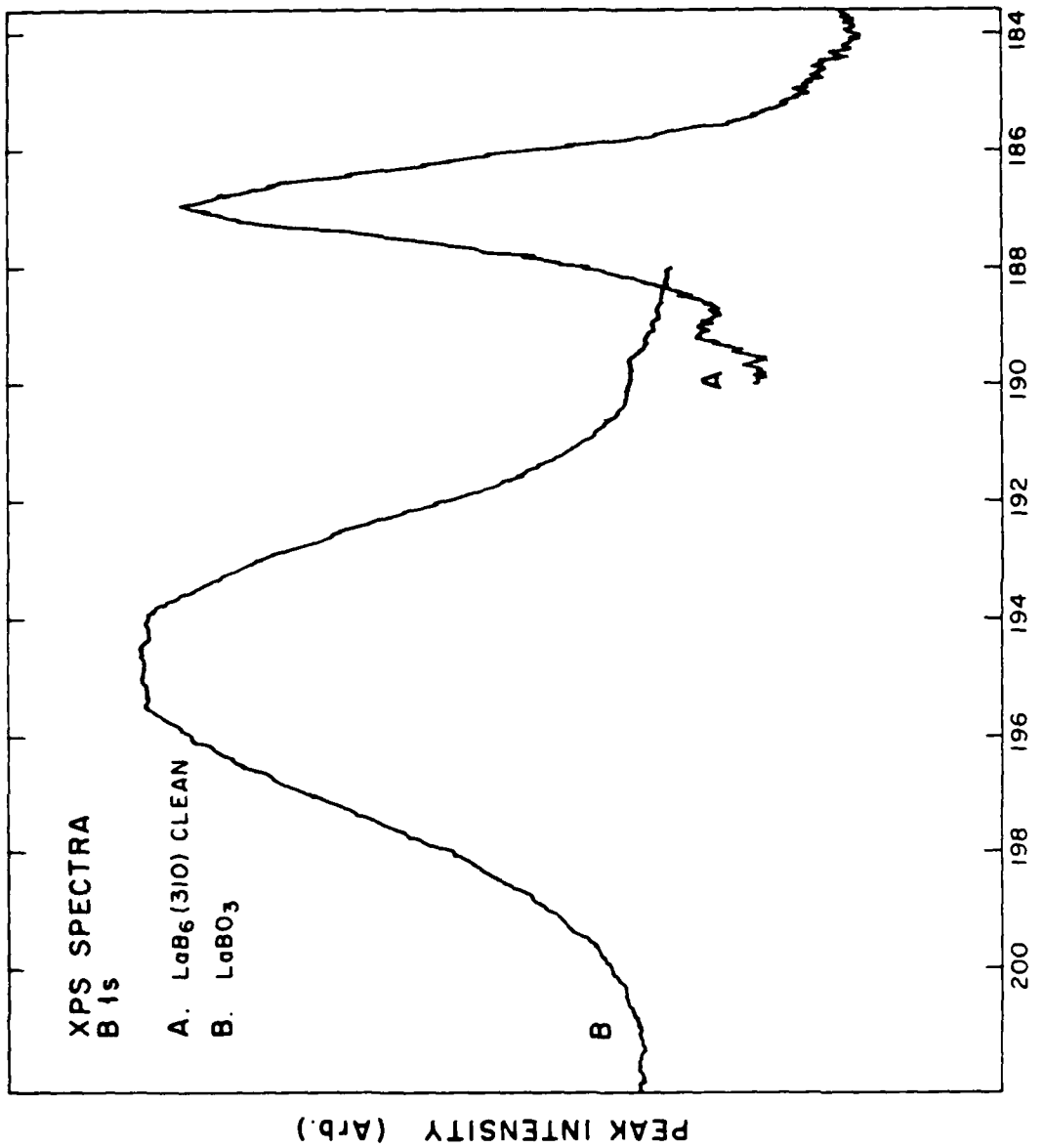

Figure 7. B 1s XPS spectra from clean LaB_6(310) and from $LaBO_3$.

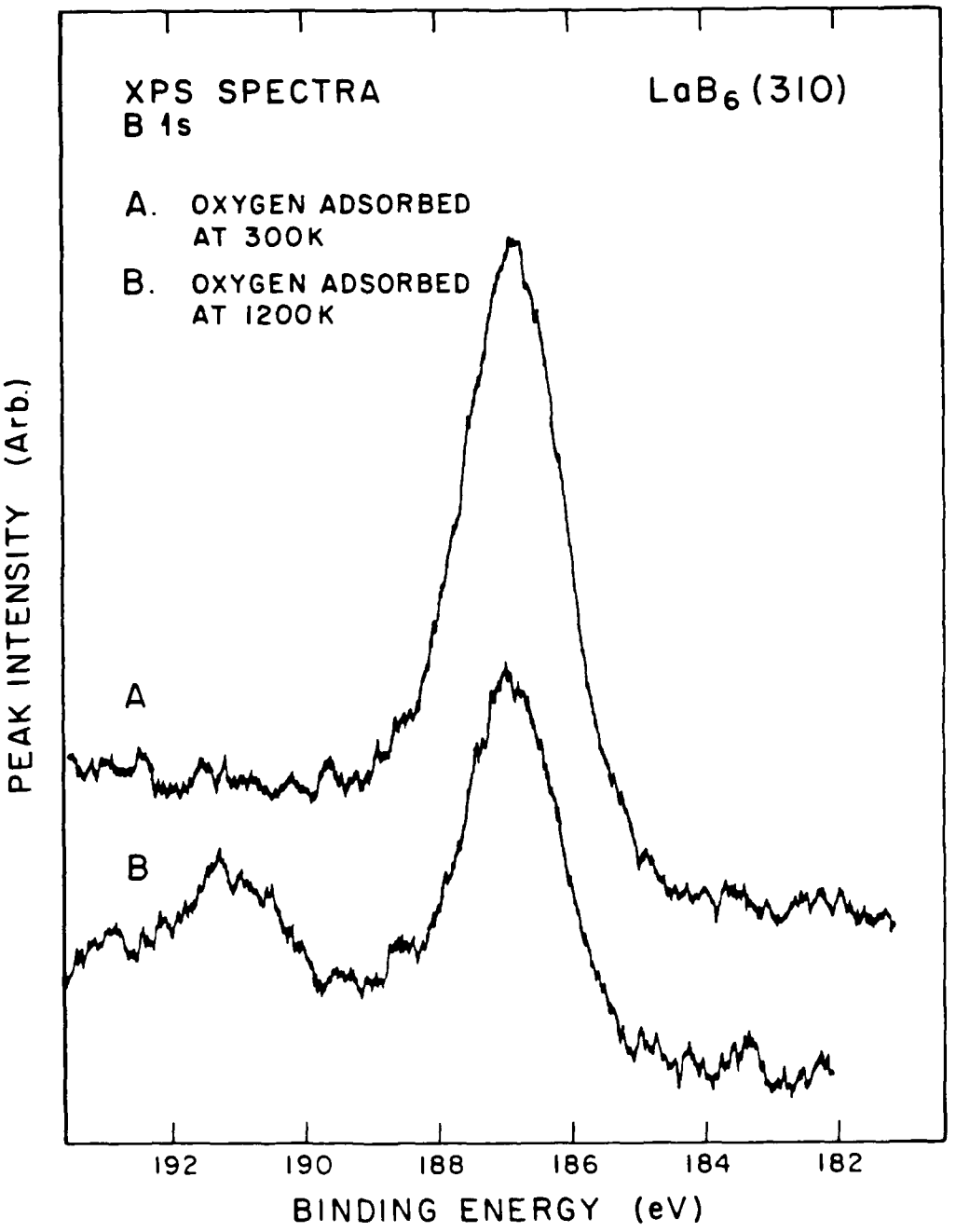

Figure 8. B 1s XPS spectra from LaB_6(310) with oxygen adsorbed at two different temperatures.

peak (Figure 8). Taken together these results show the formation of well-defined B-O and La-O binding states during heating of LaB_6 in O_2, which are not formed by room-temperature O_2 adsorption.

It has not been possible for us to identify precisely the oxide or oxides formed by heating LaB_6 in O_2. An interesting observation is that the O1s spectrum of oxidized LaB_6 is sharper (containing only a single peak) than those for La_2O_3, $LaBO_3$ and room-temperature adsorbed O_2 on LaB_6. This result suggests a single, well defined binding state for oxygen on the surface thus prepared, and multiple states for the other surfaces. This conclusion is remarkable, since splitting of both the La and B peaks is observed for this surface, suggesting oxidation of both these species.

2) Desorption results

Table IV summarizes the results of our mass spectrometric observations of desorption products from the O_2-treated LaB_6(310) surface. (All the molecules desorbed from the surface as neutrals and were ionized in the mass spectrometer. Observed ions are recorded in Table IV.) The oxygen-bearing boron species observed were BO, B_2O_2 and B_2O_3, while the only oxygen-bearing lanthanum species seen was LaO. All the molecules indicated were observed following both low and high temperature adsorption. That is, both an adsorbed monolayer of O_2 and an actual oxide layer produced the same desorption products. However, there were significant differences in desorption energies and relative amounts of the individual species for these two cases. These differences are demonstrated clearly in the thermal desorption spectra and temperature-dependent AES surface composition studies.

TABLE IV

THERMAL DESORPTION OF OXIDES FROM LAB_6(310): SPECIES MONITORED

Mass	Species	Detection Conditions	Comments
11	B^+	T ~ 1800 K clean or with adsorbed 0	Lower temperature peaks observed from fragmentation of boron oxides
27	BO^+	Observed after any oxygen exposure	Lower temperature peak observed after exposure of 1L; dominant B oxide desorbed
43	BO_2^+	Not observed	
54	$B_2O_2^+$	Observed after any oxygen exposure	
69.5	La^{++}	Same as La^+	
70	$B_2O_3^+$	Seen after oxygen exposure of > 10L	
139	La^+	T ~ 1700 K clean or with adsorbed 0	Shows fragmentation peak from LaO with adsorbed oxygen
155	LaO^+	Observed after any oxygen exposure	
326	$La_2O_3^+$	Not observed	

Figure 9 shows thermal desorption spectra of boron containing species from the surface following monolayer O_2 adsorption at room temperature. All these species in this case are first observed at 1000 K but reach their maxima at different temperatures. B_2O_3 reaches its maximum desorption rate at 1140 K with a secondary shoulder at 1300 K, where B, BO and B_2O_2 have desorption rate maxima. The peak seen at 1600 K in the B_2O_3 curve can be attributed to doubly ionized La, since the mass spectrometer resolution is insufficient to separate these two ions. Similarities in the desorption curve shapes of B and B_2O_2 in the temperature range 1200-1500 K suggest that at least some of the observed B comes from fragmentation of B_2O_2 in the mass spectrometer ionizer. The

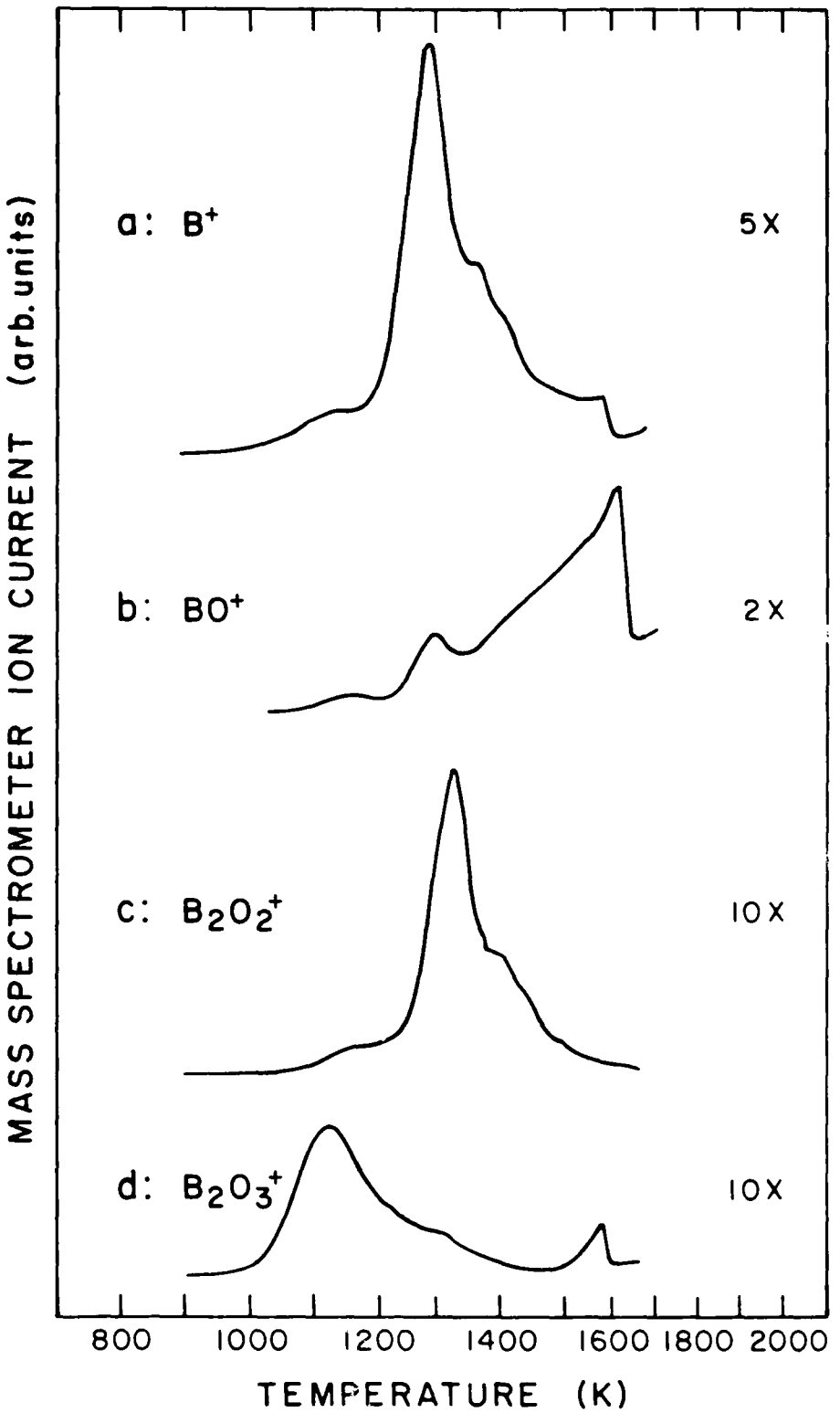

Figure 9. Thermal desorption of boron species from LaB_6(310) after an oxygen exposure of 7×10^{-5} torr-sec at 300 K. Curve a: B; curve b: BO; curve c: B_2O_2; curve d: B_2O_3. The vertical amplification factor for each curve is indicated and is consistent with other desorption spectra given here.

shoulders of the B and BO curves at 1650 K are probably related in the same fashion. While the overall mass spectrometer sensitivities are not precisely known for the various boron-oxygen molecules observed here, it is clear that BO is the dominant boron containing desorption product from a room temperature adsorbed monolayer of O_2 on a LaB_6(310) surface.

Desorption spectra of lanthanum bearing products following monolayer O_2 adsorption at room temperature are shown in Figure 10. As a comparison, the BO desorption spectrum of Figure 9 has been included. There is no apparent desorption of either La or LaO from the surface until 1500 K, at which point the desorption rates for both species increase rapidly with temperature. This increase ends only after all O_2 has desorbed from the surface. Similarities between the La and LaO desorption again suggest that La is a fragmentation product of LaO. The high temperature tails seen on most curves in this and the preceding figure are from a source other than the sample surface since no O_2 is present at the surface at temperatures above 1650 K.

Figure 11 shows the changes in surface composition observed with AES during a desorption sequence corresponding to Figures 9 and 10. Auger derivative mode peak-to-peak heights are plotted in the figure, allowing a comparison of changes in relative magnitudes of the various components. These results must be interpreted with care, since the different Auger electron energies correspond to different escape depths, meaning that slightly different depths into the surface are probed for the three species. Furthermore, derivative peak-to-peak amplitudes are not strictly proportional to the actual number N(E) of Auger electrons ejected, since changes in the shape of the N(E) peak may affect the derivative peak-to-peak amplitude considerably. Nevertheless, significant structure is present in the boron and oxygen curves, which correlates reasonably well with the multiplicity of peaks

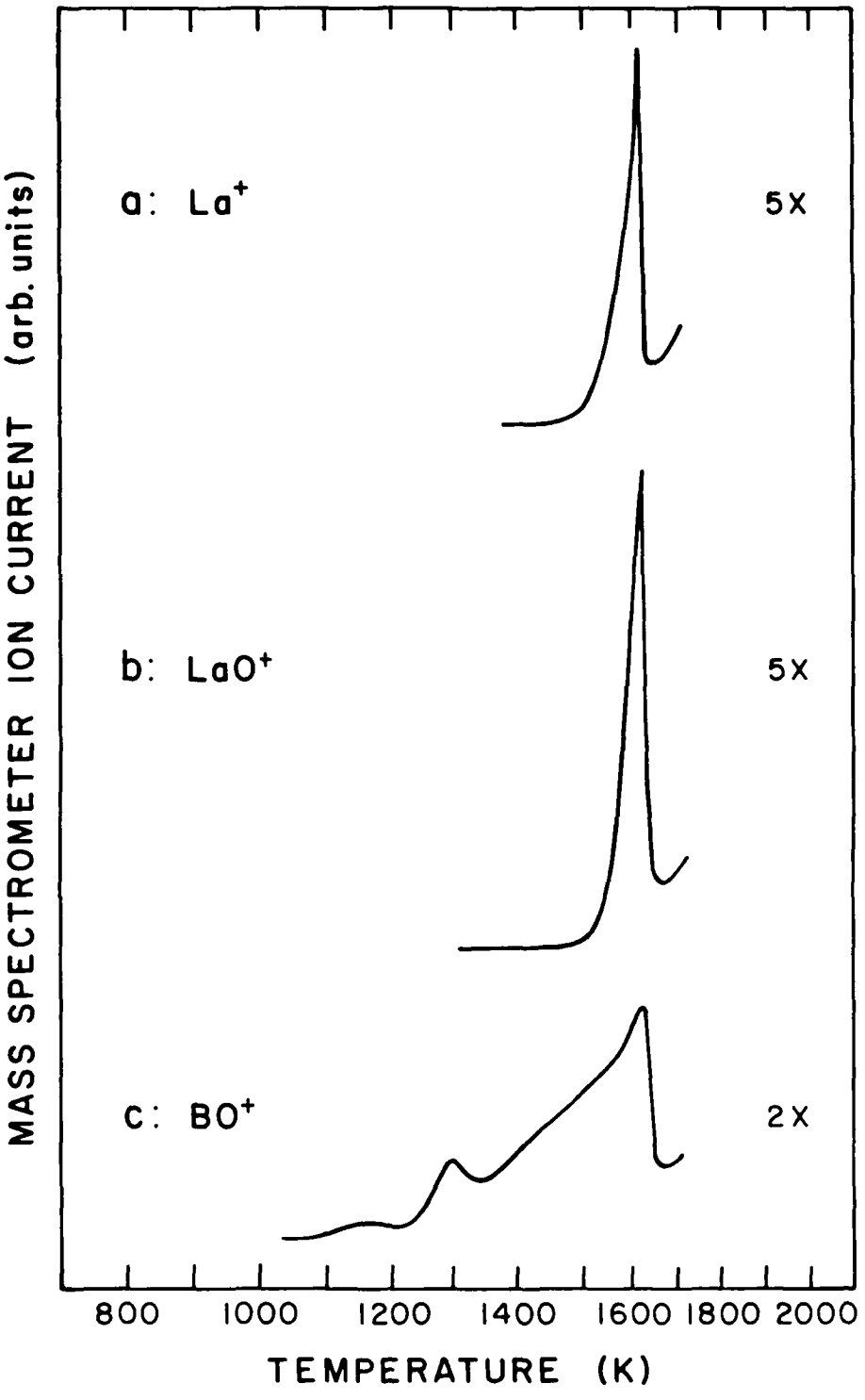

Figure 10. Thermal desorption of lanthanum species from LaB_6(310) after an oxygen exposure of 10^{-4} torr-sec at 300 K. A boron oxide species from a slightly less oxygen exposure (7×10^{-5} torr-sec) is shown for comparison. Curve a: La; curve b: LaO; curve c: BO.

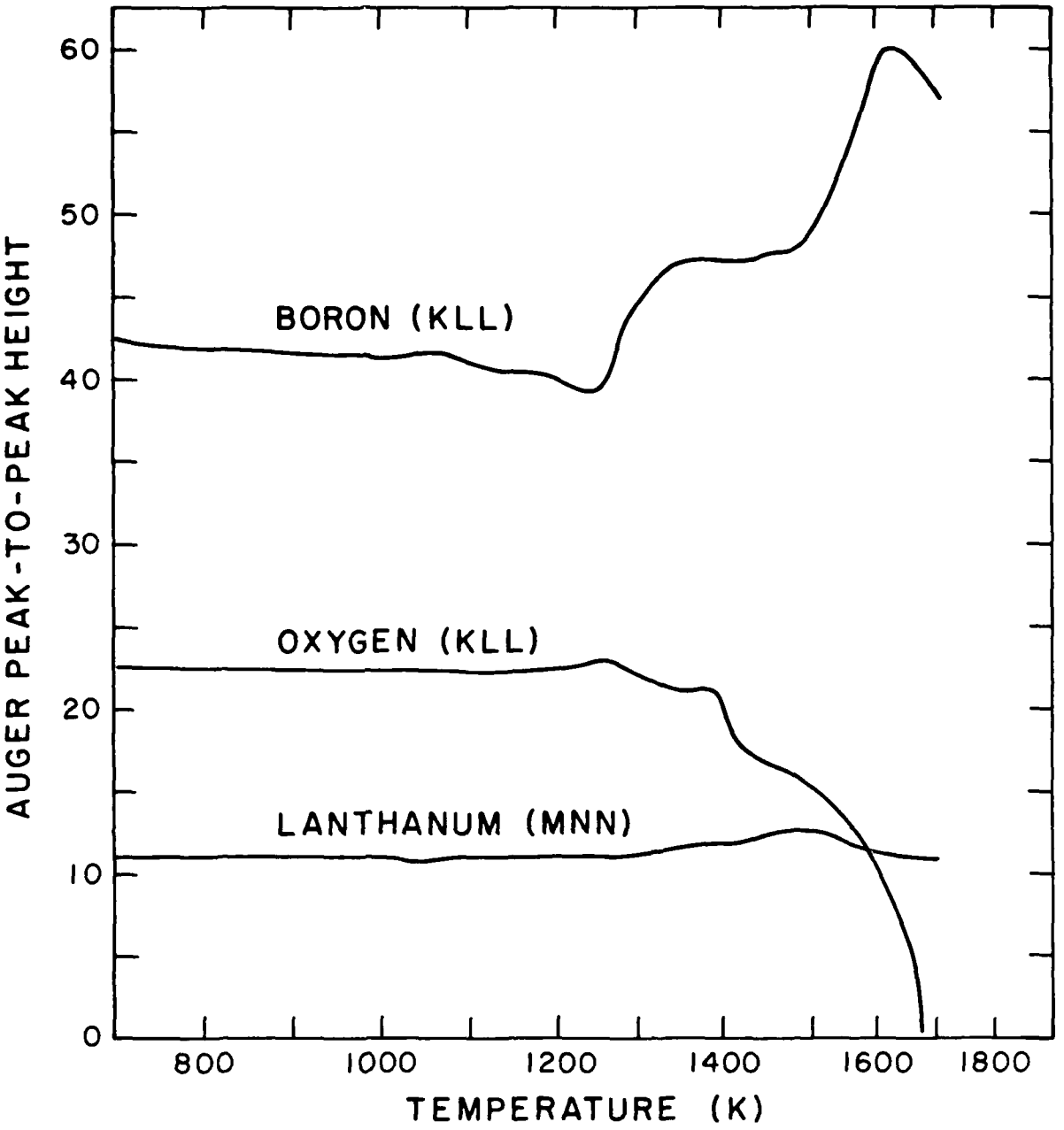

Figure 11. Variation with temperature of boron, oxygen, and lanthanum Auger peak-to-peak heights of LaB_6(310) after an oxygen exposure of 1.2×10^{-4} torr-sec at 300 K.

seen in the desorption spectra of these species. Little structure is seen in the corresponding lanthanum amplitude. Oxygen completely disappears from the surface at around 1650 K.

The effect of high-temperature oxidation of the surface, as opposed to the room temperature O_2 adsorption just discussed, is evident in the thermal desorption spectra of Figure 12, which followed heating the specimen in 1×10^{-6} torr O_2 at 1600 K for 20 min. Sharp peaks occurring at 1550 K are evident in the BO and B_2O_2 spectra, followed by a small peak at 1620 K which appears in all the desorption curves. Finally, another large sharp peak in all of the desorption curves is observed at 1700 K. This is the temperature at which most of the desorption occurs. Again, the most prominent boron species is BO.

Figure 13 shows the effect of desorption upon the composition of the oxidized surface prepared at 1600 K. Some changes in the surface are evident at temperatures below 1000 K, although most of the changes in composition occur above 1400 K. Again, little variation is seen in the lanthanum peak. Oxygen desorption from the oxidized surface is not complete until T ~ 1750 K.

The results given in Figures 9-13 show clearly the difference in character of adsorbed oxygen monolayers and high-temperature oxidized surfaces. In the latter case, not only is the oxygen more tightly bound to the boron and lanthanum atoms, as indicated by the true oxide character of the XPS and AES spectra discussed earlier, but the oxide species themselves are more strongly bonded to the surface. Thus, the desorption spectra are shifted toward higher temperature. Furthermore, a greater total amount of oxygen, present as oxide species, is bound up in the surface region. Under appropriate conditions of temperature and O_2 pressure (say ~ 1300-1600 K and 1×10^{-6} torr), it is possible to grow visible white oxide layers of at least

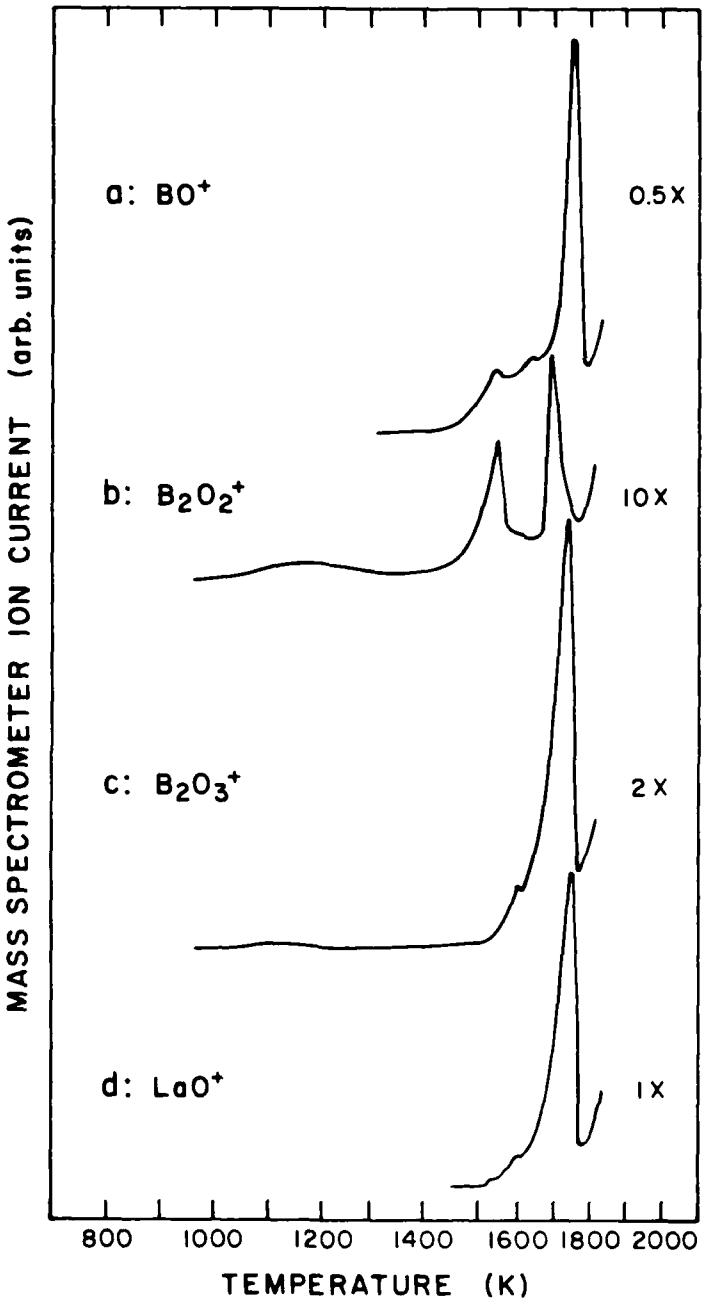

Figure 12. Thermal desorption of oxide species from LaB_6(310) after an oxygen exposure of 1.2×10^{-3} torr-sec at 1600 K. Curve a: BO; curve b: B_2O_2; curve c: B_2O_3; curve d: LaO.

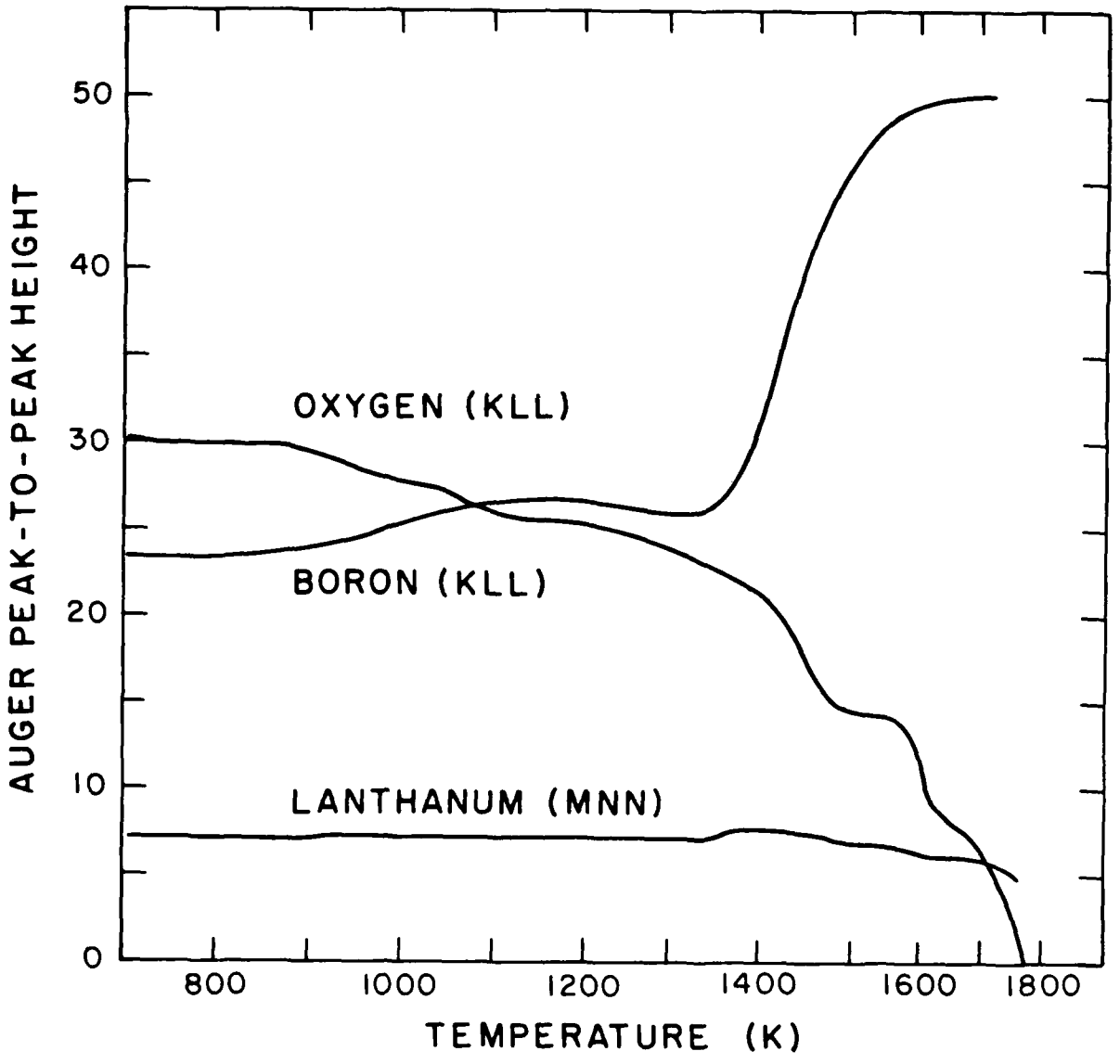

Figure 13. Variation with increasing temperature of boron, oxygen, and lanthanum Auger peak-to-peak heights of LaB_6 after an oxygen exposure of 2×10^{-3} torr-sec at 1600 K.

tens of μm (that is, many thousands of monolayers) thickness.

A final consideration in the desorption studies was to determine the evolution of species during heating in O_2. One might expect a considerably different distribution of desorbing species with temperature under these conditions as compared with those observed by oxidizing the surface and then desorbing the oxide resident on the surface. Species desorbed during heating constitute, in some sense, the complement of the oxide remaining on the surface. Thus, monitoring of desorption products during oxidation at some temperature T, followed by thermal desorption in vacuum of the species remaining on the surface, should provide a complete accounting of all oxide species produced during the oxidation. Some problems arise, however. To begin with, quantitative determination of amounts of the various species is not possible in our experiment, due to uncertainties in relative sensitivities. Also, detection of free oxygen atoms or molecules desorbed from the surface is not feasible because of the O_2 background pressure during oxidation. Therefore, a quantitative mass balance is not possible. Nevertheless, some qualitative conclusions may be drawn.

Figure 14 shows relative desorption yields of boron and lanthanum species from the $LaB_6(310)$ surface during heating in O_2 at 2×10^{-7} torr, the temperature being increased slowly to approximate steady-state conditions. A comparison with Figure 9, where O_2 was adsorbed at room temperature and then desorbed in vacuum shows strikingly different behavior. In the temperature range up to ~ 1500 K, B_2O_2 appears to be the dominant boron desorption product during heating in O_2. Figure 9, on the other hand, shows significant contributions from BO and B_2O_3 desorption from preadsorbed oxygen layers in this temperature range. It seems possible that a direct reaction between O_2 molecules and surface boron is kinetically favored in this temperature range

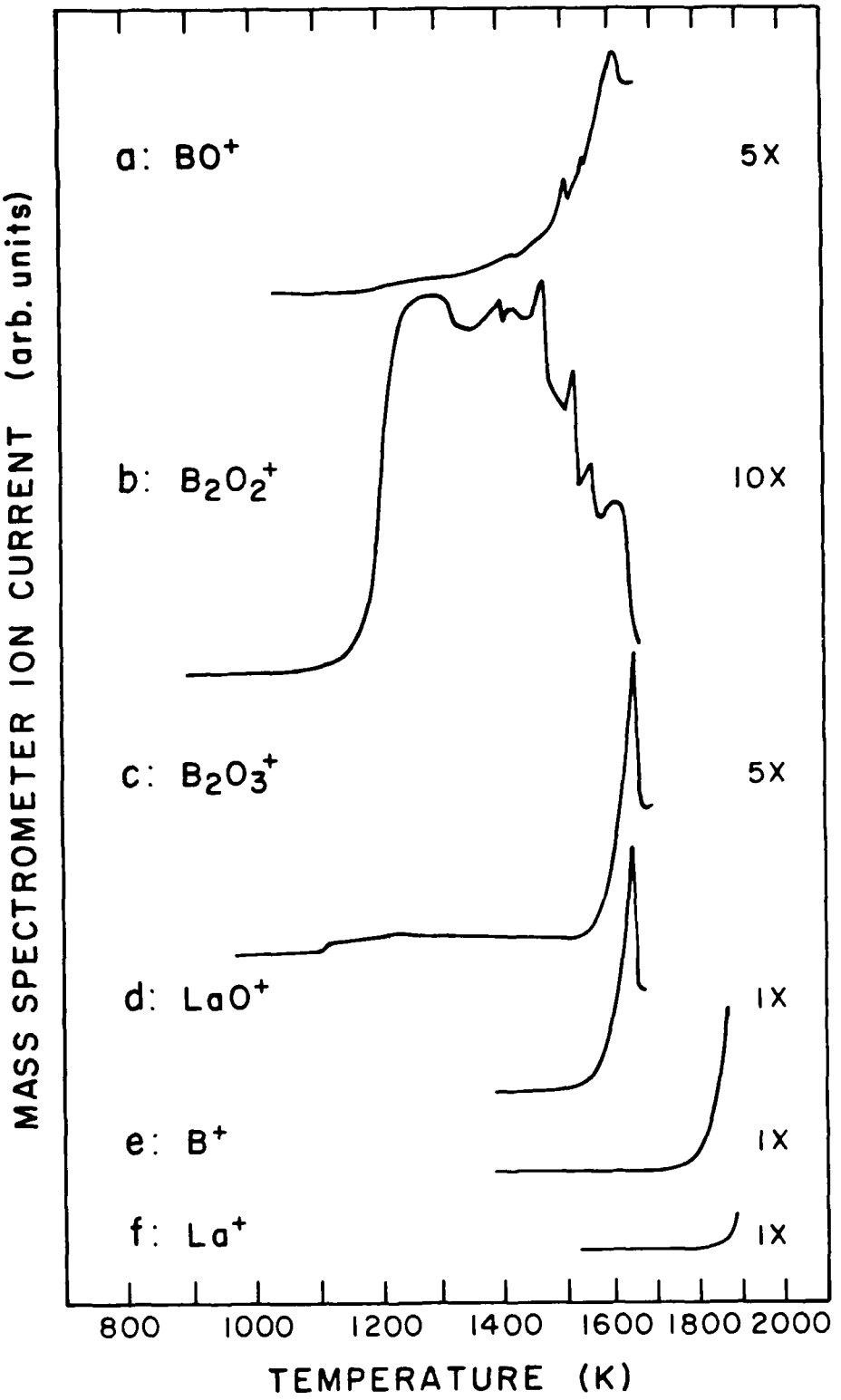

Figure 14. Relative desorption yields of BO, B_2O_2, B_2O_3, and LaO from LaB_6(310) as a function of increasing temperature in an oxygen pressure of 2×10^{-7} torr. Yields of B and La (curves e and f) from the clean surface are included for comparison.

at steady O_2 pressures, thereby producing more B_2O_2.

Only at temperatures exceeding 1500 K is desorption of lanthanum-containing species ever observed, whether in steady O_2 pressures or in vacuum. Therefore, the surface stoichiometry is clearly changed by heating in O_2 at T < 1500 K, due to preferential boron removal. Excess lanthanum thus produced is tied up in the adsorbed oxide phase discussed earlier.

The results presented here are similar to those reported for the LaB_6(100) face [15], with the major exception that the B_2O_2 peak was always larger than the BO peak for adsorbed and oxidized layers on the (100) face, while the BO peak dominates on the (310) face. Furthermore, the shape of the B_2O_3 spectrum differs for the two surfaces. These differences are especially interesting because the (310) surface studied here was found to be faceted to (100) steps by the experiments described here. We expect that this faceting occurred rather early in the course of these studies, since initial experiments involved extended heating in O_2 for mass spectrometer optimization and calibration. Thus, the desorption spectra reported here are most likely characteristic of a surface of (100) steps rather than a single (310) surface. It is well known that surface reaction products and their rates of formation may differ considerably between smooth surfaces and step edges, so there could be significant differences in desorption spectra between the (100) surface studied earlier [15] and that discussed here.

The most convenient comparison between the results of the present study and other investigations of LaB_6 surface reactions with O_2 may be made on the basis of desorption energies of mass spectrometrically observed species. These energies are commonly calculated by a technique devised by Redhead [20] which requires only a knowledge of desorption peak temperature and the rate of sample temperature increase in the experiment. Thus reliable comparisons

between results of different investigators may be made. Table V summarizes results of this and other studies.

TABLE V

THERMAL DESORPTION OF OXIDES FROM LaB_6: BINDING ENERGIES

Species	Binding Energy (eV)[a]		
	$LaB_6(310)$[b]	$LaB_6(100)$[c]	$LaB_6(110)$[d]
BO	4.7 + 0.2	3.6 ± 0.1 4.3 ± 0.1	3.4 3.9 4.1
B_2O_2	3.7 ± 0.1	3.3 ± 0.1 3.5 ± 0.1	-
B_2O_3	3.34 ± 0.1	3.4 ± 0.1	-
LaO	4.6 ± 0.1	4.3 ± 0.2	4.2

[a] determined by the Redhead method
[b] after oxygen adsorption at 300 K
[c] from reference [15]; after oxygen adsorption at 1000 K
[d] from reference [17]; after oxygen adsorption at 300 K

Significant differences in BO and LaO binding energies between the present results (steps of (100) orientation) and the flat (100) surface results are obvious in Table V. The higher binding energy of LaO in the present work may be explained by stoichiometry differences. The sample used here had a precise stoichiometry of $LaB_{6.09}$, yielding a lower La volatility than that of the $LaB_{5.74}$ specimen used for the (100) studies. We suspect that the onset of LaO desorption is related to the desorption of La itself, so that increasing the binding energy of La to the surface may also increase the desorption energy of LaO. Thus, the higher desorption energy of LaO observed here is not surprising. The reason for higher BO desorption energy is not clear, but is probably related to the presence of steps on the surface.

It should be noted that in the present study an interesting phenomenon was observed following high temperature oxidation of the surface. The desorption energies of all the observed species shifted to higher temperature as the sample was oxidized at higher temperature. That in itself is not surprising, since weakly bound species should desorb during the oxidation itself. However, it was observed that oxidation at 1600 K in 1×10^{-6} torr O_2 produced desorption peaks around 1700 K (~ 4.9 eV) for all the observed species. It is not possible to determine in these experiments whether this result means that tightly bound forms of all the observed molecules exist on the surface in this case, or whether a single oxygen-containing species is present which decomposes around 1700 K, releasing oxygen which immediately reacts to form the other desorption products.

E. Task III(A): Investigations of clean Mo-oxide surfaces

Surfaces of so-called sublimed Mo-oxide samples have been studied as TEC collector electrodes. These samples were prepared by Thermo Electron Corporation, Waltham, MA. A typical specimen consists of a 70-100 μm layer of partially oxidized Mo, deposited onto a Nb or Ni substrate by heating a Mo filament in vacuum with a controlled partial pressure of O_2. The resultant porous layer contains 1000-15000 ppm oxygen, as determined by bulk chemical analysis.

We have studied three such samples, using AES and XPS and have done a comparative study of a 1100 ppm O sample and an 8000 ppm O sample using XPS. Figure 15 shows splitting of the Mo 3d doublet in these Mo-oxide surfaces, compared with the sample spectrum for a clean polycrystalline Mo surface. Note that peaks characteristic of metallic Mo, as well as an oxidized state, are observed on the Mo-oxide. (These two types of peaks overlap and cannot be resolved with the CRISS instrument in its present state. Future upgrading of

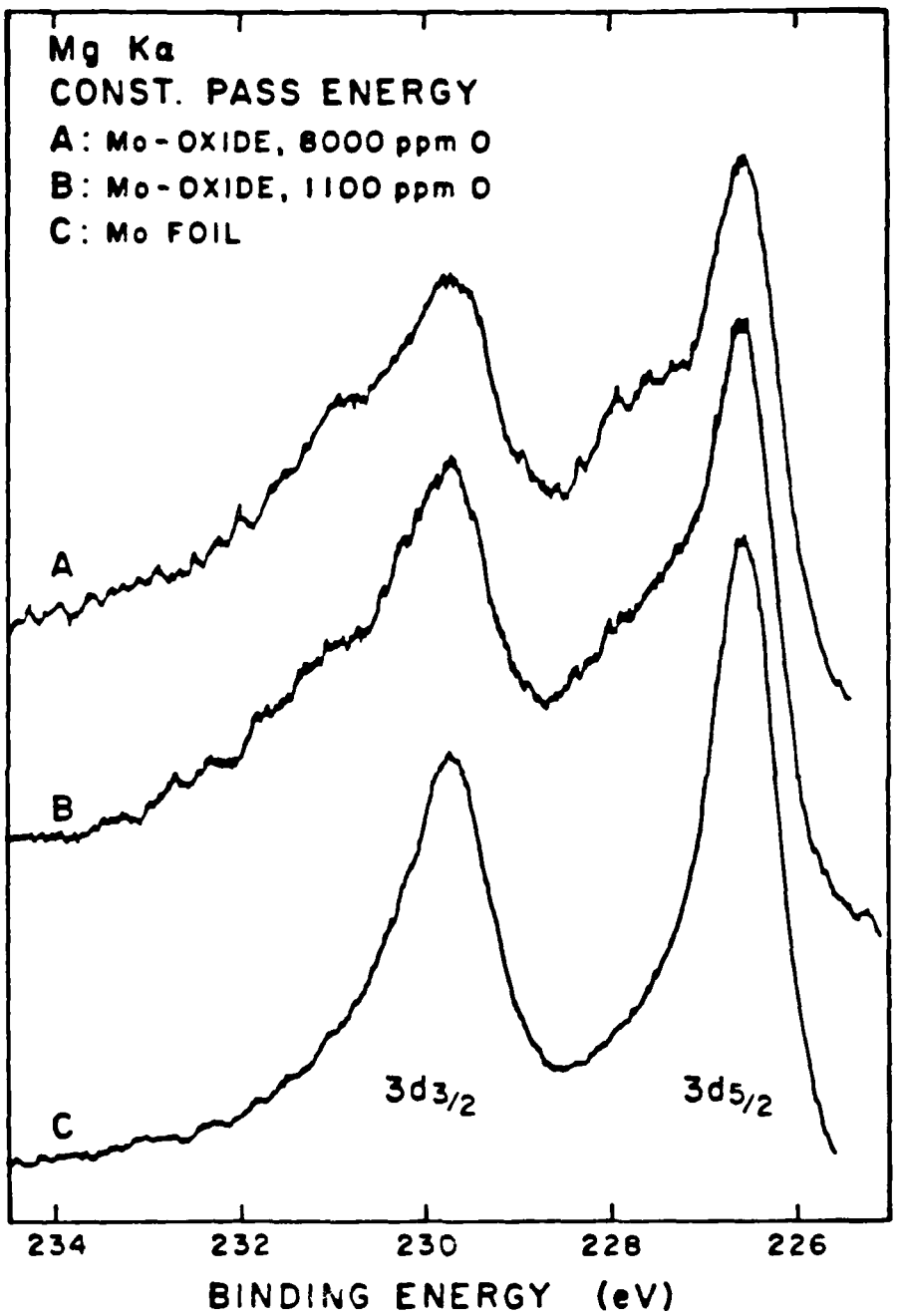

Figure 15. Broadening of the Mo 3d doublet due to oxygen. XPS data obtained using Mg Kα radiation. A,B: Mo-oxide specimens. C: Clean Mo foil.

this system is expected to include a beam monochromator for improving the resolution.)

The energy shift expected between Mo^0 and Mo^{6+} oxidation states (i.e., between metallic Mo and MoO_3) is ~ 5 eV, while the shift between Mo^0 and Mo^{4+} (MoO) is about 1.5 eV [21]. The shift we have observed for Mo-oxide specimens, compared with clean Mo, is ~ 1.4 eV, suggesting an oxidation state of Mo^{4+}. Such a result is not unreasonable for the highly substoichiometric Mo-oxide specimens, which contain 1100-8000 ppm (0.1-0.8 wt %) O_2. Pure stoichiometric MoO_3, on the other hand, contains about 33 wt % O_2. Note, however that the half-width of the low kinetic energy (high binding energy) tail on the Mo-oxide peaks is nearly twice the size of that on the Mo peaks, suggesting that some oxidation states higher than Mo^{4+} may be present.

A comparison of Mo-oxide surfaces heated in vacuum and in O_2 has been made, using XPS. Results indicate that the surface concentration of oxygen on Mo oxide specimens may be reduced to levels approaching those on thermally cleaned polycrystalline Mo foil, and that the initial Mo-oxide surface layer may be restored by heating to 1100 K for a few seconds in air. This reversibility may be very useful in preparing Mo-oxide collectors with precisely controlled Cs adsorption properties.

F. Task III(B): Investigations of Cs adsorption on Mo-oxide surfaces

A typical Mo-oxide surface consists of a layer of molybdenum sublimed, in a controlled oxygen atmosphere, onto a metallic substrate, such as polycrystalline molybdenum or nickel. The particular specimen used in this study has a 5 mil thick coating, containing about 11,000 ppm oxygen, on a Ni substrate. This sample was equipped with a W-5% Re/W-26% Re thermocouple for precise measurement of temperature in the range below 1000 K.

Initial studies focused upon the change in FERP work function with Cs

coverage of the Mo-oxide surface. Postoperational analysis of a Mo-oxide collector which had been used in a test converter [22] showed Cs to be present throughout the oxide layer. The "clean" work function, i.e., the work function of the surface after heating to 1150 K, was ~ 3.7 eV. This relatively low value resulted from the presence of residual Cs in the bulk and on the surface. We have found that the work function of a Mo-oxide surface which has not been exposed to Cs is ~ 6.0 eV.

In the postoperational study mentioned [22], additional Cs was adsorbed on the starting surface in an effort to determine the minimum attainable work function. These results are shown in Figure 16. We have performed similar measurements on an initially clean (no Cs) surface. The data thus obtained are plotted in Figure 17. Note that work function is given as a function of Cs Auger signal, normalized to oxygen Auger signal. This method of presenting the data results in a slightly non-linear abscissa, but provides a direct measure of coverage, allowing both adsorption and desorption experiments to be performed. The data of Figure 17 were actually taken by adsorption of Cs to saturation at room temperature (Cs/O ≃ 0.5) and then heating in steps to remove Cs from the surface. After each heating step, the sample was cooled and FERP and AES measurements were made. The points in the range near Cs/O ≃ 0.1 correspond to the "residual" Cs remaining on the surface after heating to 1150 K for a few seconds, the most vigorous heat treatment used in these studies.

We believe this sequence of adsorption/heating corresponds more closely to actual converter operation than does a simple adsorption experiment. However, it is interesting to compare the maximum work functions of our sample (~ 4.5 eV after 1150 K) and that studied at TECO [22], (~ 3.7 eV after 1150 K) following Cs adsorption studies. This comparison, in conjunction with AES

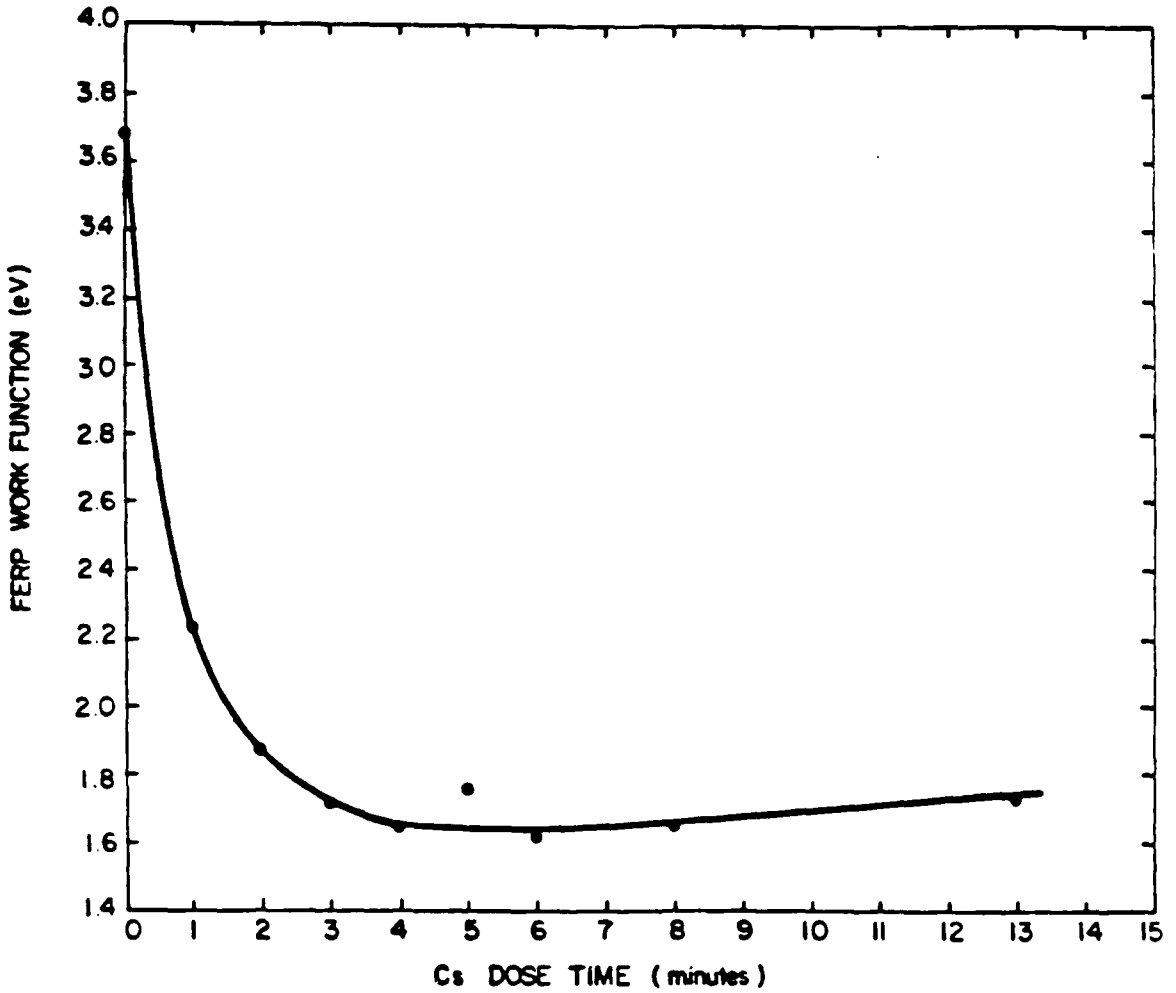

Figure 16. FERP work function vs Cs dose time at constant rate. Results from Ref. 22 for a sublimed Mo-oxide collector previously used in a test converter.

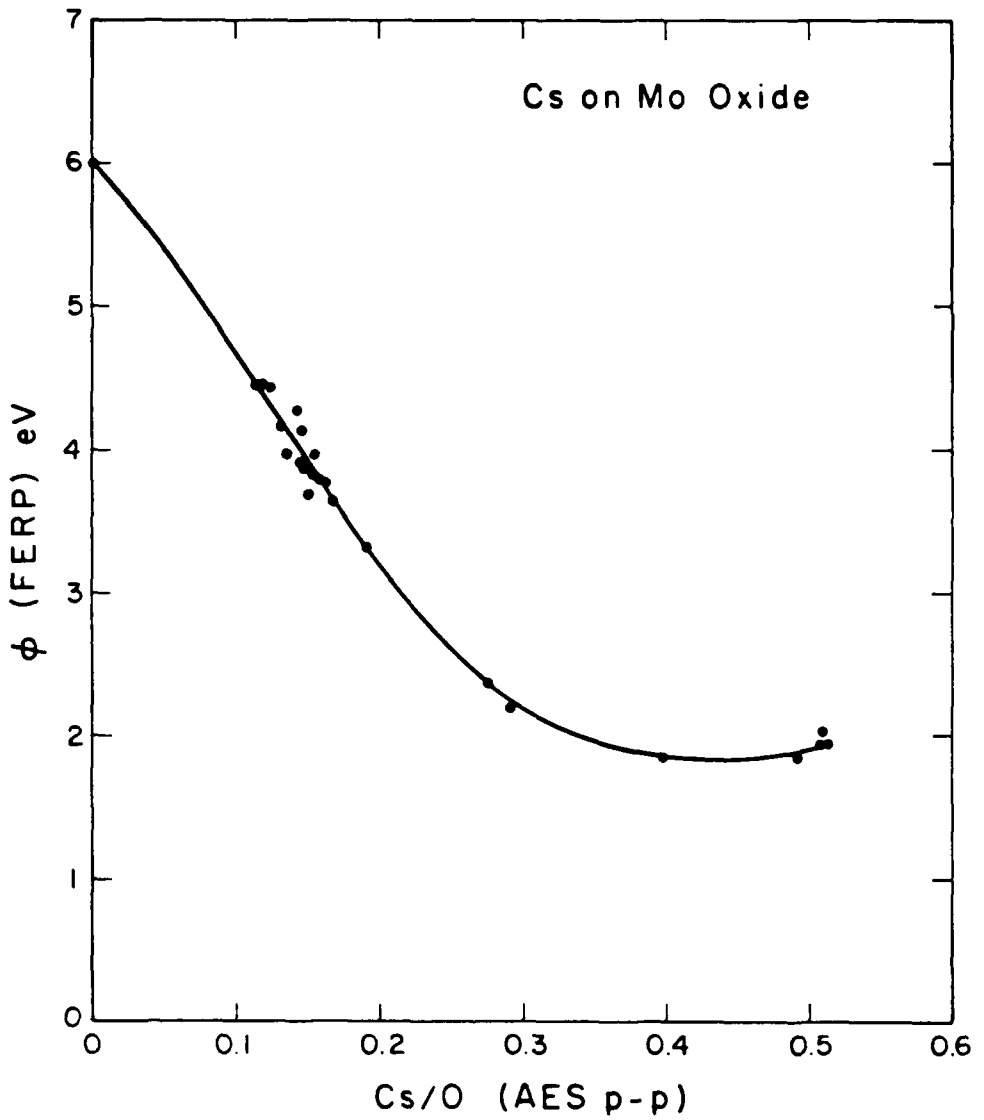

Figure 17. FERP work function vs Cs coverage of sublimed Mo-oxide surface, expressed as Cs/O AES peak-to-peak ratio. Cs was adsorbed to saturation, then removed by heating in steps.

results, indicates that the collector actually used in a converter is saturated with more Cs than our sample, a very reasonable result. Thus, our measurements indicate an early state in the Cs saturation (activation) of a Mo-oxide collector.

An interesting effect has been noted in these FERP experiments, a phenomenon which we have not observed on other surfaces. This effect is a broadening of the energy distribution of collected FERP electrons during a particular range of the heating cycle following Cs adsorption. In order to understand the nature of this effect, it is necessary to see how the FERP energy distribution is determined. Figure 18(A) shows a derivative-mode peak of collected FERP electrons, corresponding to a sweep of collector potential from a value where no electrons are collected (V_c < 1.6 volts) to a value where nearly all the incident electrons are collected (V_c ≈ 2.4 volts). Since the curve is a derivative, it represents the slope of the I vs V_c curve of collected current. The steepness of the leading edge, given as the 10% - 90% value, is a measure of the width of the collected electron energy distribution, 145 meV for curve A. Curve A corresponds to optimum sharpness of the observed distribution, with the width resulting from the finite Fermi-Dirac energy distribution of field emitted electrons at 300 K and instrumental broadening by the electron optical system of the FERP gun. For most surfaces, FERP 10% - 90% values in the range 150 - 175 meV are routinely observed.

Curve B in Figure 18 is a broadened FERP distribution, with a 10% - 90% value of 250 meV. This peak corresponds to a higher work function and is thus shifted relative to Curve A. Possible reasons for such broadening will be discussed later.

Broadened FERP peaks are observed in the Cs/Mo-oxide system when the Cs-saturated surface is heated in small temperature increments. Figure 19 shows

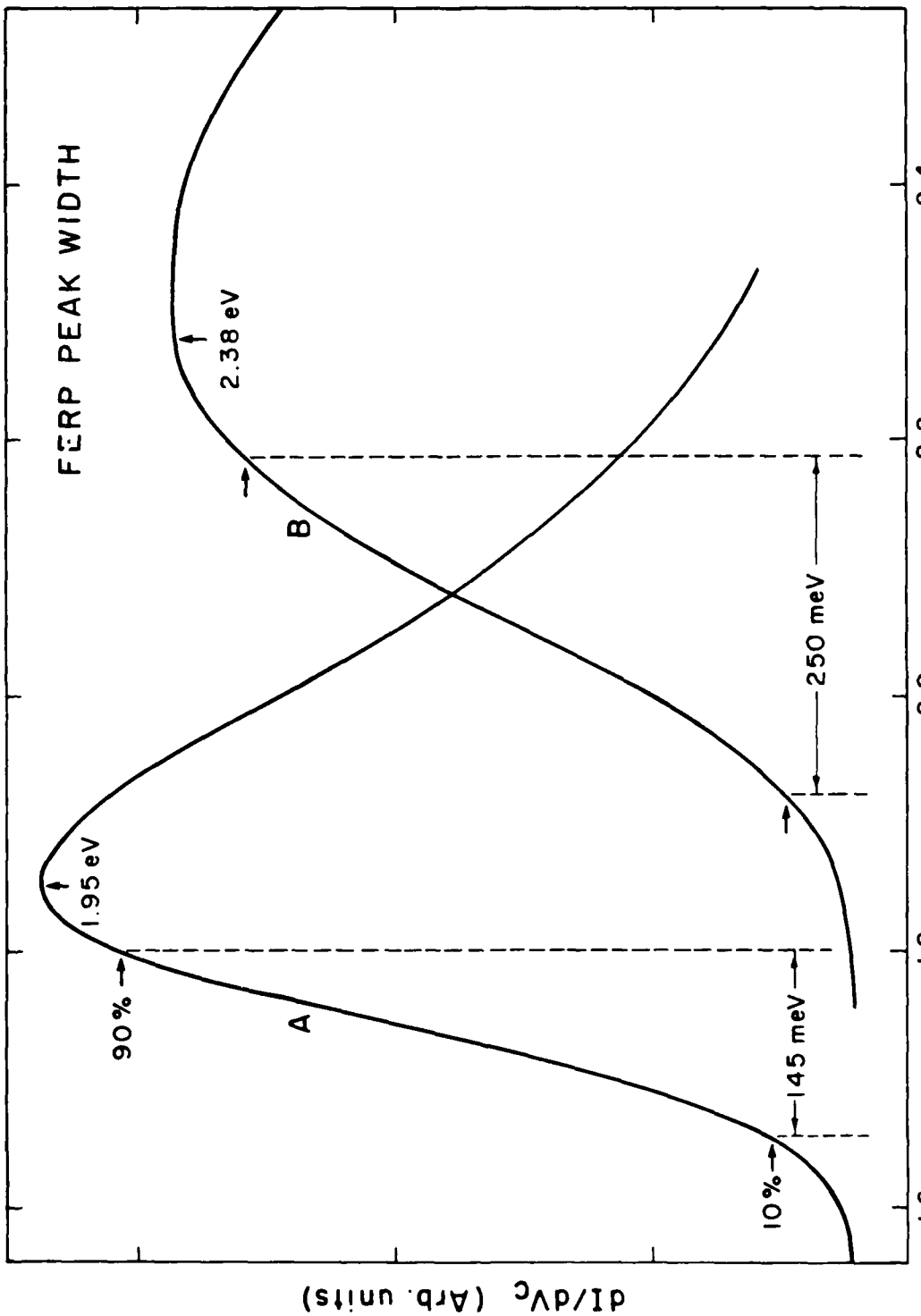

Figure 18. Normal (A) and broadened (B) FERP peaks, observed for the system Cs/Mo-oxide.

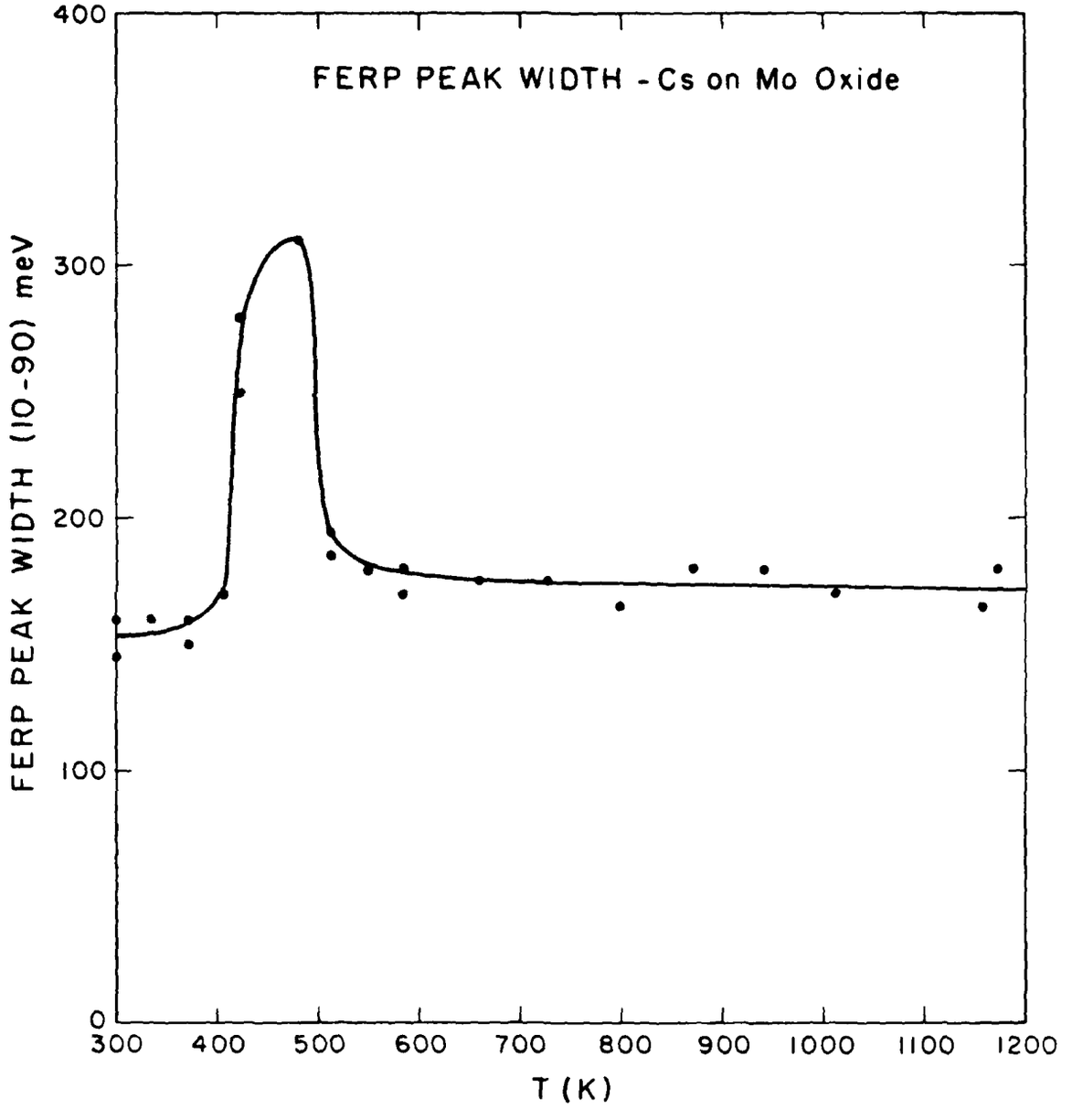

Figure 19. FERP peak width vs heating temperature, starting with a saturated Cs layer on Mo-oxide. Following each heating step, the sample was cooled to room temperature before making the FERP measurement.

the FERP peak width (10% - 90%) as a function of heating temperature for the Mo-oxide surface initially saturated with Cs. Following each heating step, the surface was cooled to room temperature before making the FERP measurement. Thus, the peak broadening observed in the range 400-500 K is due to a change in the surface, induced by heating, which remains after the sample is cooled.

A surface parameter which obviously may change during heating is the Cs coverage, so the removal of Cs from the surface by heating was studied in small temperature steps. Figure 20 is a summary of change in Cs/O AES ratio and work function with heating. Note that Figures 19 and 20 result from the same set of experiments. That is, the ϕ values in Figure 20 and the 10% - 90% values in Figure 9 came from the same FERP measurements. Also, both figures consist of data from several runs. Therefore, the behavior of the FERP peak width is reproducible from run to run.

A careful comparison of Figures 19 and 20 shows that the anomalously broad FERP peaks are observed in the heating range 400-500 K, the region where the largest changes in Cs coverage and work function are observed. Thus, broadening of the FERP peak seems to be associated with an intermediate Cs coverage or with changes occurring during removal of Cs from the surface.

Broadening of the FERP peak observed in past experiments has generally been attributed either to surface patches with different work functions, or to a large electron reflection coefficient near the Fermi energy. Since the Mo-oxide used here is polycrystalline, different work function patches are very likely. On the other hand, Cs diffusion into the bulk is also known to occur, which could possibly alter the reflection coefficient. Thus, the precise cause of the FERP peak broadening cannot be determined from these experiments.

Desorption from the system Cs/Mo-oxide was studied by mass spectrometry. The intent was to determine whether Cs oxides were desorbed, or whether only

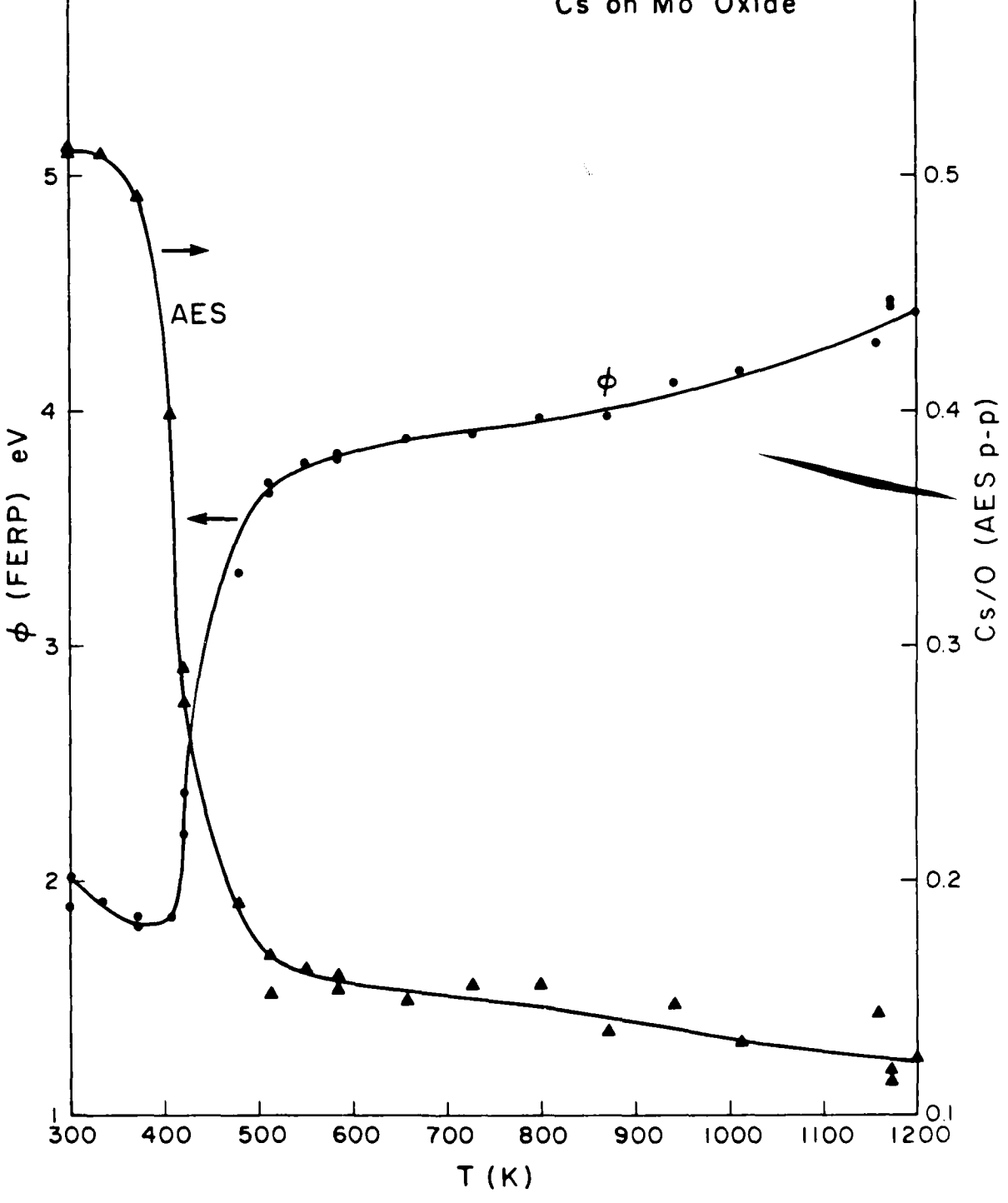

Figure 20. Work function and Cs/O AES ratio during heating sequence for initially saturated Cs layer on Mo-oxide. The data are from the same set of measurements used in Figure 19.

metallic Cs was desorbed during heating of the cesiated surface. It had been suggested previously that desorption of Cs oxides might explain the appearance of an emitter "oxygen effect" in test converters using Mo-oxide collectors.

Table VI shows the neutral species for which desorption was investigated, for temperatures in the range $300 \leq T \leq 1200$ K. Note that none of these species was observed. Thus, within the detectability limit of our spectrometer (estimated to be ~ 10^{-4} monolayer/sec for Cs) no neutral desorption occurred. During the same heating, however, the surface coverage of Cs decreased dramatically, as determined by AES and verified by FERP, as already discussed. This result suggested rapid diffusion of Cs into the Mo-oxide bulk, in agreement with postoperational analyses of Mo-oxide collectors done by Danielson [22], which showed Cs distributed throughout the Mo-oxide.

TABLE VI

THERMAL DESORPTION OF NEUTRALS FROM Cs/Mo-OXIDE, $T < 1200$ K

Species*	Detected?	Comments
Cs	No	Desorption of Cs^+ ions from surface observed for proper sample bias (see text)
Cs_2	No	
Cs_2O	No	
CsO	No	

*Estimated Cs detection limit ~ 10^{-4} monolayer/sec

We have also investigated the desorption of Cs^+ ions from the surface, by biasing the sample slightly positive and shutting off the QMS filament. Such desorption is to be expected when T is high enough and the surface work

function is higher than the first ionization potential of Cs. According to the Saha-Langmuir equation, we should have

$$I^+/I_o = (g_+/g_o) \exp[(\phi - I)/kT] \quad (1)$$

where I is the Cs ionization potential and g_+ and g_o are constant statistical weights.

We expect, for first order desorption,

$$I_o = C_o \sigma \exp(-E_o/kT) \quad (2)$$

with C_o the rate constant, σ the Cs surface coverage, and E_o the neutral desorption energy. Since the Cs coverage changes very little for heating above ~ 600 K, we consider σ constant for this discussion. Thus,

$$I^+ = (C_o \sigma g_+/g_o) \exp[(-E_o - I + \phi)/kT] \quad (3)$$

and

$$(d \ln I^+/d\, 1/T) = (-E_o - I + \phi)/k. \quad (4)$$

We know the value of I to be 3.89 eV for Cs. Furthermore, if we make the assumption that the surface work function, for heating above ~ 800 K, is not a function of T, then we may plot ln I^+ vs 1/T and find $-(E_o + \phi)$ from the slope, m. Thus,

$$m = [\phi - (E_o + I)]/k \quad (5)$$

$$\text{or } E_o = \phi - km - I \quad (6)$$

Figures 21 and 22 show such plots for Cs^+ desorption after 5 and 15 two min. Cs doses, respectively. These plots yield km values of -3.32 eV and -2.86 eV, respectively. The work function results discussed earlier suggest that heating above ~ 800 K reduces the Cs coverage to a value yielding a work function of 4.0-4.5 eV. Substituting these numbers and the ionization potential of Cs gives $2.97 \leq E_o \leq 3.93$ eV.

Part of the broad range of variation of E_o is undoubtedly due to changes in ϕ and km with changes in residual Cs coverage. Nevertheless, the neutral

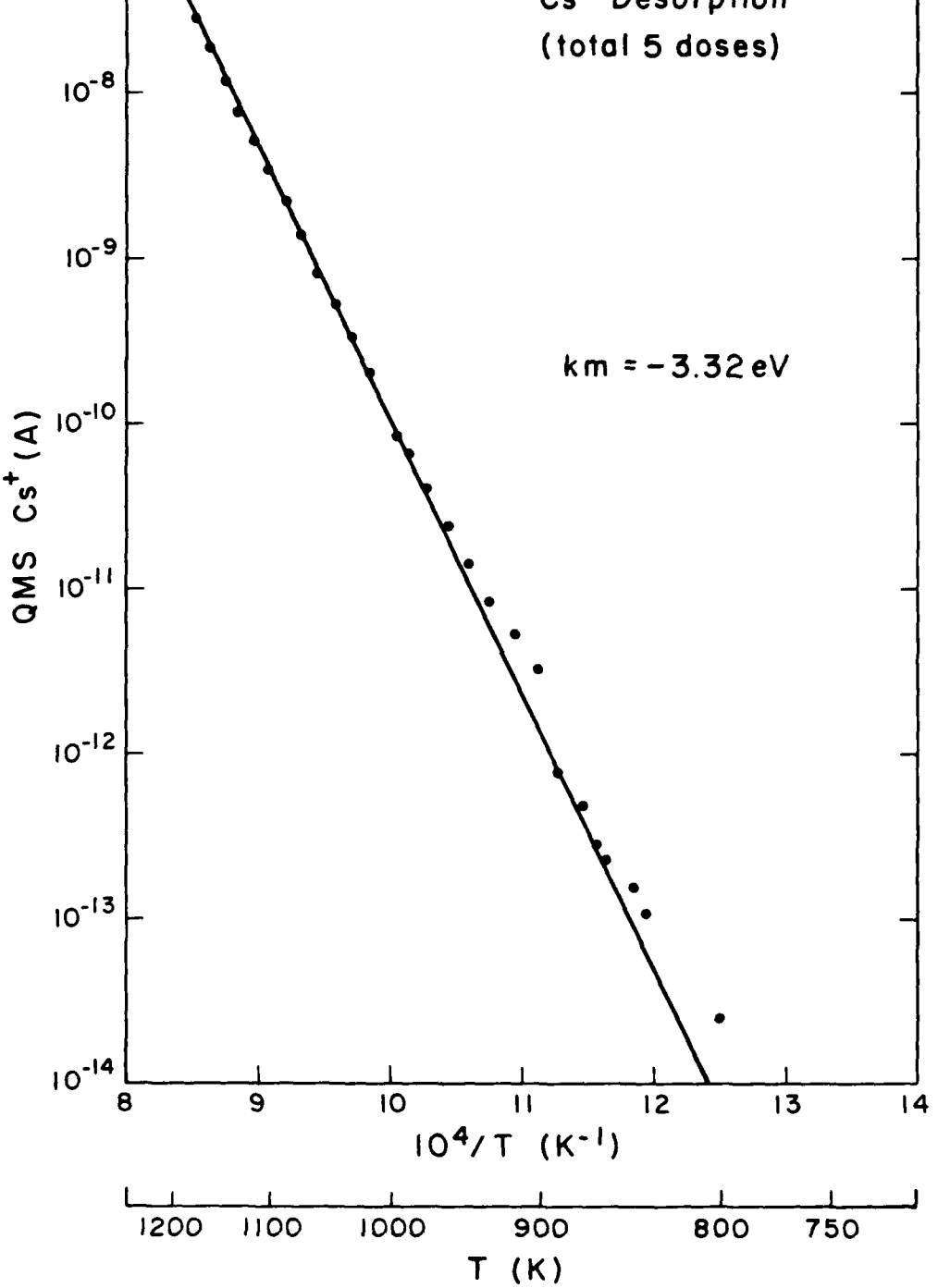

Figure 21. Cs^+ desorption from Mo-oxide after 5 Cs doses.

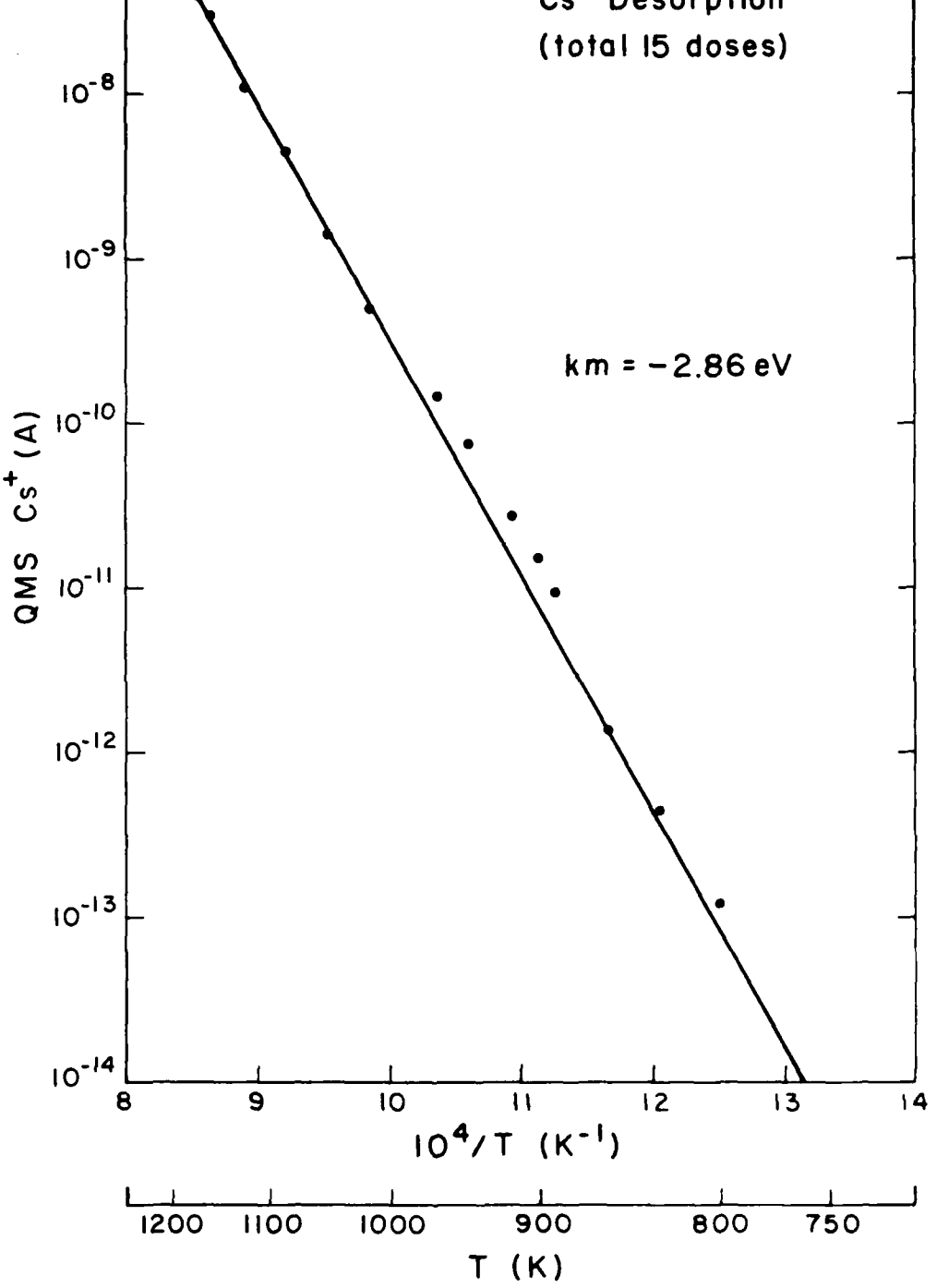

Figure 22. Cs^+ desorption from Mo-oxide after 15 Cs doses.

desorption energy is greater than ~ 3 eV, a reasonably high value for Cs desorption. It is thus easy to explain, qualitatively, why diffusion occurs rather than desorption: the activation energy for diffusion of Cs into the Mo-oxide layer is apparently less than the neutral desorption energy. Thus, diffusion is the energetically easiest path for the Cs atom to take.

Data presented earlier, Cs AES signal vs T, should allow us to calculate the activation energy for Cs diffusion into the Mo-oxide. We assume a behavior of the form

$$-d\sigma/dt = D = \nu\sigma\exp(-E/kT) \qquad (7)$$

where D is the rate of diffusion, σ is the coverage, ν is a pre-exponential factor and E is the diffusion activation energy. This equation is identical in form to the equation for first-order thermal desorption [20]. Our model is thus equivalent to "desorption" from the surface into the oxide bulk and obviously assumes a negligible bulk concentration of Cs throughout the process. Since we know that we have not come anywhere near saturation of the oxide with Cs, even after multiple Cs doses, the assumption of negligible concentration seems to be reasonable.

We wish to find, approximately, the energy required for the last Cs atom to diffuse into the bulk, as this energy is likely to be the greatest, in analogy with the terminal desorption energy for thermal desorption. Thus, we expect to get an upper limit on the activation energy for diffusion.

We proceed as follows: Integration of Eq.(7) over a narrow range ($\sigma_i \rightarrow \sigma_f$) yields, upon rearrangement,

$$\ln(\ln\ \sigma_i/\sigma_f) = -E/kT + \ln\ \nu + \ln(\Delta t) \qquad (8)$$

where Δt is the time interval over which the desorption takes place. If σ_i and σ_f are close in value and the time over which the "desorption" takes place is short, the left hand side and the $\ln(\Delta t)$ term on the right hand side of

Eq.(8) can be neglected. Equation (8) then reduces to,

$$E \simeq kT \ln \nu. \qquad (10)$$

From Figure 20, we see that the reduction in surface coverage due to diffusion is essentially complete at 500 K. Furthermore we assume the pre-exponential factor to be of order 1×10^{13}, as assumed by Redhead [20] and thus arrive at an upper limit for the diffusion activation energy of E = 1.3 eV, significantly lower than the neutral desorption energy of ~ 3 eV calculated above. We thus have a plausible explanation for the experimental observation that Cs diffuses into the Mo-oxide bulk rather than desorbing as neutral atoms.

G. Task IV: Construction and use of in situ test system

An initial aim of this project was the construction, testing and use of a system which would allow converter electrodes to be surface analyzed in situ, without exposure to atmosphere, following operation in a test converter. This facility was to be used in collaboration with other investigators in order to provide rapid information on surface phenomena occurring at real electrode surfaces during converter operation. This facility was actually constructed during the project, but it was not used for its intended purpose, since very little practical converter research was done in other laboratories during the tenure of this grant. We therefore concentrated our effort on the study of single crystals and other model surfaces which have already been discussed. The details of the design and construction of the in situ test system have been thoroughly discussed in earlier reports.

H. Task V: Construction and use of ARAES system

An angle-resolved Auger electron spectroscopy (ARAES) system has been constructed and is being used for the study of surface phenomena occurring at a LaB_6(110) surface. The design of this system is very similar to that of an

earlier system, also built in our laboratory, which was used to study O_2 adsorption onto the LaB_6(100) surface, as has been discussed in detail elsewhere [5]. The earlier system was built using funds from another source, and has moved with its builder to the University of Minnesota. Our second generation system has been used primarily by J. DeLord and R. Martin (see Section V, Interactions) as an undergraduate research facility for advanced students from Reed College and Lewis and Clark College, although it is physically located at OGC. Much of the effort has gone into improvements in signal-to-noise ratio of the data acquisition system and into data handling software development. This system has provided undergraduate research projects for 6 students to date.

REFERENCES

1. P. R. Davis and G. A. Schwind, Appl. Surf. Sci. 25 (1986) 355.
2. L. W. Swanson, M. A. Gesley and P. R. Davis, Surf. Sci. 107 (1981) 263.
3. M. Gesley and L. W. Swanson, Surf. Sci. 146 (1984) 583.
4. P. R. Davis, L. W. Swanson, J. J. Hutta and D. L. Jones, J. Mat. Sci. 21 (1986) 825.
5. S. A. Chambers and L. W. Swanson, Surf. Sci. 131 (1983) 385.
6. V. N. Shrednik, Sov. Phys.-Solid State 3 (1961) 1268.
7. R. A. Collins and B. H. Blott, Surf. Sci. 10 (1968) 348.
8. L. W. Swanson and L. C. Crouser, J. Appl. Phys. 40 (1969) 4741.
9. L. R. Danielson and L. W. Swanson, Surf. Sci. 88 (1979) 14.
10. P. R. Davis, Surf. Sci. 91 (1980) 385.
11. D. W. Tuggle and L. W. Swanson, J. Vac. Sci. Technol. B3 (1985) 220.
12. Yu. M. Goryachev, I. A. Podchernyaeva, N. I. Siman, V. S. Sinel'nikova, I. I. Timofeeva and G. S. Burkhanov, Sov. Phys.-Tech. Phys. 23 (1978) 321.
13. G. Haufler and H. Goretzki, Proc. 1970 Thermionic Conversion Specialist Conf. (Oct. 26-29, 1970, Miami, FL).
14. E. Storms and B. Mueller, J. Appl. Phys. 50 (1979) 3691.
15. P. R. Davis and S. A. Chambers, Appl. Surf. Sci. 8 (1981) 197.
16. R. Nishitani, S. Kawai, H. Iwasaki, S. Nakamura, M. Aono and T. Tanaka Surf. Sci. 92 (1980) 191.
17. E. B. Bas, P. Hafner and S. Klauser, in: Proc. 7th Intern. Vacuum Cong. and 3rd Intern. Conf. Solid Surfs. (Vienna, 1972) 881.
18. C. Oshima, T. Tanaka, R. Nishitani and S. Kawai, J. Appl. Phys. 51 (1980) 997.
19. G. Hanke and K. Muller, J. Vac. Sci. Technol. A2 (1984) 964.

20. P. A. Redhead, Vacuum 12 (1962) 203.

21. C. D. Wagner, W. M. Riggs, L. E. Davis, J. F. Moulder and G. E. Muilenberg, Handbook of X-Ray Photoelectron Spectroscopy (Perkin-Elmer Corporation, Physical Electronics Division, Eden Prairie, MN, 1979).

22. Progress Report No. 48, DOE Contract DE-AC02-81ET11291 (Thermo Electron Corp., Sept. 1981).

III. Publications

Table VII is a comprehensive list of articles published, in press or being prepared for publication in scientific journals as a result of the research effort reported here.

TABLE VII

PUBLICATIONS

1. S. A. Chambers an L. W. Swanson, "Angle-Resolved Auger Electron Emission from LaB_6(001) with and without Chemisorbed Oxygen," Surf. Sci. 131 (1983) 385.
2. M. Gesley and L. W. Swanson, "A Determination of the Low Work Function Planes of LaB_6," Surf. Sci. 146 (1984) 583.
3. L. W. Swanson and P. R. Davis, "Work Function Measurements," in Methods of Experimental Physics. Vol. 22, Solid State Physics-Surfaces (Academic Press, New York, 1985, ed. R. L. Park and M. G. Lagally), p. 1.
4. D. W. Tuggle and L. W. Swanson, "Emission Characteristics of the ZrO/W Thermal Field Electron Source," J. Vac. Sci. Technol. B3 (1985) 220.
5. P. R. Davis, L. W. Swanson, J. J. Hutta and D. L. Jones, "Fabrication and Characterization of Rare Earth Hexaboride Single-Crystal Materials," J. Mat. Sci. 21 (1986) 825.
6. P. R. Davis, G. A. Schwind and L. W. Swanson, "The Effect of Oxygen Pressure on Volatility and Morphology of LaB_6 Single Crystal Cathodes," J. Vac. Sci. Technol. B4 (1986) 112.
7. P. R. Davis and G. A. Schwind, "Low Work Function Emitter Electrodes for Advanced Thermionic Converters," Appl. Surf. Sci. 25 (1986) 355.
8. K. D. McKinstry and P. R. Davis, "Interaction of Oxygen with a LaB_6(310) Surface," (in preparation, to be submitted to Surf. Sci.).

9. P. R. Davis, "XPS Studies of the Zr/O/W(100) Surface," (in preparation, to be submitted to Surf. Sci.).

10. P. R. Davis, M. A. Gesley, L. W. Swanson and J. J. Hutta, "Comparison of Thermionic Cathode Parameters of Low Index Single Crystal Faces of LaB_6, CeB_6 and PrB_6," (in preparation, to be submitted to Appl. Surf. Sci.).

IV. Personnel Associated with Research Effort

A. Personnel

Table VIII is a cumulative list of personnel of the OGC Surface Physics Group who have been associated with this research project. Other collaborators outside OGC are listed in Section V: Interactions.

TABLE VIII

RESEARCH PERSONNEL

Paul R. Davis, Associate Professor (Principal Investigator)

Lynwood W. Swanson, Professor (Co-investigator)

Gregory A. Schwind, Senior Research Associate

Stuart Palmiter, Research Technician

Mark Petteys, Research Technician

Mark A. Gesley, Ph.D. Student

Michael J. Bozack, Ph.D. Student

William Mackie, Ph.D. Student

Locke Christman, Ph.D. Student

Kevin D. McKinstry, M.S. Student

B. Degrees Granted

Several of the students listed above have completed their degree requirements and been awarded degrees. The details are given below.

Michael J. Bozack

Ph.D. in Applied Physics awarded January, 1985

Thesis title: "Surface Phenomena in Liquid Metal Alloys with Application to Development of a Liquid Metal Source of B and As"

Dr. Bozack is currently doing postdoctoral research in surface science at the University of Pittsburgh.

Mark A. Gesley

Ph.D. in Applied Physics awarded June, 1985

Thesis title: "Spectral Analysis of Field Emission (1/f) Noise"

Dr. Gesley is currently employed in a research group at IBM Corp., Yorktown Heights, NY.

Kevin D. McKinstry

M.S. in Applied Physics awarded September, 1985

Thesis title: "Interaction of Oxygen with a LaB_6(310) Surface"

Mr. McKinstry is currently living in Colorado.

V. Interactions (coupling activities)

A. Collaborations

1. DoD collaborations

Partly as a result of the work reported here, we currently have two LaB_6(310) cathodes under test at the Air Force life test facility at Rome Air Development Center, Griffiss AFB, NY. Testing of these cathodes is a cooperative effort between OGC and RADC personnel. Initial test data, after about 3000 hours of life, were reported at the 1986 Tri-Service Cathode

Workshop, held at RADC. The cathodes are now approaching 8000 hours of operation, and are still functioning normally.

2. Non-DoD collaborations

We have worked in cooperation with faculty members of three local colleges on research connected with this project. W. Mackie, who is working in collaboration with Prof. C. Hinrichs at Linfield College (an undergraduate institution in McMinnville, OR), is also a Ph.D. student within the OGC Surface Physics Group. He has been studying the preparation and field emission properties of TiC and ZrC at Linfield, and will continue to investigate surface properties of these materials in his Ph.D. research here at OGC. L. Christman, a recent graduate of Linfield who worked on TiC and ZrC single crystal fabrication there, has also joined our group as a Ph.D. student.

The second area of collaboration has been on the angle-resolved AES (ARAES) experiment. Professors J. DeLord of Reed College and R. Martin of Lewis and Clark College (both located in Portland, OR) have cooperated with the OGC Surface Group in development and operation of this experiment. The experimental apparatus is housed at OGC and consists of equipment from a variety of sources, including a special specimen manipulator constructed with AFOSR funding, a Reed College vacuum system and specially modified Auger analyzer, and various other components supplied by OGC, Reed College and Lewis and Clark College. The experiment has provided hands-on experience to a number of undergraduate students from both colleges.

B. Conference papers presented

Table IX is a cumulative list of conference papers presented during the research project.

TABLE IX

CONFERENCE PAPERS

1. P. R. Davis, L. W. Swanson and M. J. Bozack, "Surface Properties of Ceramic/Metal Composite Materials for Thermionic Converter Applications," presented at 1983 IEEE International Conference on Plasma Science, May 23-25, 1983, San Diego, CA.
2. L. W. Swanson and P. R. Davis, "Single Crystal LaB_6: A Comparison with Currently Used Thermionic Cathodes for Broad Beam Applications," presented at 1983 IEEE International Conference on Plasma Science, May 23-25, 1983, San Diego, CA.
3. P. R. Davis, "Investigation of Emission and Stability Characteristics of High Index Planes of LaB_6," presented at 1984 Tri-Service Cathode Workshop, April 3-5, 1984, Washington, DC.
4. P. R. Davis, "Properties of LaB_6 Single Crystal Surfaces," presented at AFOSR Molecular Dynamics and Surface Chemistry Contractors' Conference, October 24-26, 1984, Albuquerque, NM.
5. P. R. Davis, "Surface Phenomena at Thermionic Energy Converter Electrodes," presented at 7th Symposium on Applied Surface Analysis, May 15-17, 1985, College Park, MD.
6. P. R. Davis, G. A. Schwind and L. W. Swanson, "The Effect of Oxygen Pressure on Volatility and Morphology of a LaB_6 Single Crystal Cathode," presented at 29th International Symposium on Electron, Ion and Photon Beams, May 28-31, 1985, Portland, OR.
7. P. R. Davis and K. D. McKinstry, "Interaction of Oxygen with a LaB_6(310) Surface," presented at 1985 AFOSR Surface Chemistry Contractors' Conference, November 4-6, 1985, Dayton, OH.

8. P. R. Davis, "Recent Developments in LaB_6 Cathode Technology," presented at 1986 Tri-Services Cathode Workshop, March 25-27, 1986, Rome, NY.

END

1-87

DTIC